A Novel Copper(II) Indenoisoquinoline Complex Inhibits Topoisomerase I, Induces G2 Phase Arrest, and Autophagy in Three Adenocarcinomas.

Caroline Molinaro, Nathalie Wambang, Till Bousquet, Anne-Sophie Vercoutter-Edouart, Lydie Pelinski, Katia Cailliau, Alain Martoriati

HAL Id: hal-03857606

https://hal.univ-lille.fr/hal-03857606

Submitted on 17 Nov 2022

1 # A novel copper(II) indenoisoquinoline complex inhibits topoisomerase
2 # I, induces G2 phase arrest, and autophagy in three adenocarcinomas.

3 **Caroline Molinaro [1], Nathalie Wambang [3], Till Bousquet [2], Anne-Sophie Vercoutter-Edouart [1],**
4 **Lydie Pélinski [2], Katia Cailliau [1†], and Alain Martoriati [1†*]**

5 [1]Univ. Lille, CNRS, UMR 8576-UGSF-Unité de Glycobiologie Structurale et Fonctionnelle, F-59000
6 Lille, France

7 [2]Univ. Lille, CNRS, Centrale Lille, Univ. Artois, UMR 8181-UCCS-Unité de Catalyse et Chimie du
8 Solide, F-59000 Lille, France

9 [3]Intertek, 2561 Av Georges V, H1L 6S4, Montréal, Québec, Canada

10 † These authors contributed equally to this work

11 *** Correspondence:**
12 Alain Martoriati
13 alain.martoriati@univ-lille.fr

14 **Keywords: Indenoisoquinoline, copper(II) complex, adenocarcinoma, topoisomerase, cell cycle,**
15 **autophagy.**

16 **Article type**

17 Original research article, 6,969 words, 8 figures, 3 tables, and 2 supplementary figures.

18 **Abstract**

19 Topoisomerases, targets of inhibitors used in chemotherapy, induce DNA breaks accumulation leading
20 to cancer cell death. A newly synthesized copper(II) indenoisoquinoline complex WN197 exhibits a
21 cytotoxic effect below 0.5 µM, on MDA-MB-231, HeLa, and HT-29 cells. At low doses, WN197
22 inhibits topoisomerase I. At higher doses, it inhibits topoisomerase IIα and IIβ, displays DNA
23 intercalation properties. DNA damage is detected by the presence of γH2AX. The activation of the
24 DNA Damage Response (DDR) occurs through the phosphorylation of ATM/ATR, Chk1/2 kinases,
25 and the increase of p21, a p53 target. WN197 induces a G2 phase arrest characterized by the
26 unphosphorylated form of histone H3, the accumulation of phosphorylated Cdk1, and an association
27 of Cdc25C with 14.3.3. Cancer cells die by autophagy with Beclin-1 accumulation, LC3-II formation,
28 p62 degradation, and RAPTOR phosphorylation in the mTOR complex. Finally, WN197 by inhibiting
29 topoisomerase I at low concentration with high efficiency is a promising agent for the development of
30 future DNA damaging chemotherapies.

31 **1   Introduction**

32   Adenocarcinomas are the most diagnosed cancers. Among them, breast and cervix, respectively
33 the first and fourth most represented cancers in women, and colorectal cancers the second and third
34 most represented cancers respectively in women and men [1]. Current treatments include
35 chemotherapy with agents that generate DNA damage to trigger cancer cell division arrest and
36 associated programmed cell death of tumours [2,3].

37   Topoisomerases (Top) regulate DNA topology during replication, transcription, and
38 chromosomal segregation [4–6]. To relieve torsional strain, these DNA-interacting enzymes cleave
39 one or two DNA strands before the religation step [7,8]. Human Top are subdivided into three
40 subgroups including IA (Top3α and Top3β), IB (Top1 nuclear and Top1 mitochondrial), and IIA
41 (Top2α and Top2β), type I Top cause single-strand breaks (SSB) while type II Top generate double-
42 strand breaks (DSB) [9]. In anticancer therapy, inhibition of Top allows DNA cleavage, prevents the
43 religation reaction, and leaves cancer cells with DNA breaks. Top1 and Top2 are mainly targeted due
44 to their overexpression in many cancers including breast, cervix, and colorectal cancers [10–13]. The
45 increased quantity and activity of Top in highly dividing cells directly correlate with positive responses
46 to Top inhibitory treatments [12,14,15]. The primary cytotoxic lesions in cancer cells result from
47 collisions between the trapped Top and the replication forks [16–18]. DNA breaks further trigger the
48 activation of DNA Damage Response (DDR) pathways, leading to cell cycle arrest and to death if DNA
49 damage is too severe [19,20]. The DDR pathways start with the recruitment and the phosphorylation
50 of histone H2AX on serine 139 (γH2AX) by phosphoinositide 3-kinase related kinase family members
51 ATM, ATR, and DNA-PK [21,22]. Consecutively, Chk1 and Chk2 kinases are activated, inhibit
52 phosphatase Cdc25 [23], and induce a cell cycle arrest followed in most cases by apoptosis [20].

53   Top inhibitors display different action mechanisms. Poisons target the DNA/topoisomerase
54 cleavage complex, form a ternary complex (interfacial inhibition) inhibiting DNA religation, and result
55 in persistent DNA breaks [24]. Catalytic inhibitors either intercalate into DNA in the Top fixation site
56 or are ATP competitors or hydrolysis inhibitors to provoke an antineoplastic effect [25]. A small
57 number of Top inhibitors are approved for clinical use. The Top2 poison doxorubicin and its isomer
58 epirubicin from the anthracycline family are first-line antineoplastic agents used against many different
59 types of solid tumours, leukemias, and lymphomas [26,27], with main side effects including
60 cardiotoxicity and t-AML (treatment-related acute myelogenous leukemia) [28–30]. At high doses (up
61 to 10 μM), doxorubicin becomes a DNA intercalator and contributes to increase DNA breaks [31,32].
62 Top2 poison etoposide (VP-16) also induces t-AML [9]. The Top1 poison camptothecin derivatives,
63 topotecan and irinotecan, are used to treat solid tumours including ovary, cervix, pancreatic, lung, and
64 colorectal cancers [33]. However, their use in chemotherapy is limited by their instability, the need for
65 long-term chemotherapies, and by severe side effects including hematotoxicity, vomiting and diarrhea
66 [34]. Unlike camptothecins, the Top1 inhibitors indenoisoquinolines are chemically stable, are not
67 substrates for drug efflux transporters and as such are promising Top inhibitors [35,36].
68 Indenoisoquinoline derivatives (LMP400, LMP776, and LMP744) are in phase I/II clinical trials
69 [35,36].

70   Since the discovery of platinum anticancer properties and the use of cisplatin, a platinum-based
71 alkylating agent, and its derivatives in chemotherapy [37–39], other metal-based drugs have been
72 designed and developed for their cytotoxic effects on tumour cells [40–42]. Transition metals from the
73 d-block of the periodic table (groups 3 to 12) [43–46] are particularly suitable for this purpose as they
74 adopt a wide variety of coordination geometries [47]. Among them, copper modifies the backbone of
75 the complexed ligand and grants better DNA affinity [48–50]. Copper derivatives interact with DNA
76 using noncovalent interactions with the major or the minor DNA grooves, intercalation, or electrostatic
77 binding to enhance DNA damage, and display antitumour activity [51]. Some copper complexes inhibit
78 either or both Top1 and Top2 and results in severe DNA damage, cell cycle arrest, and death in cancer
79 cells [52,53].

80   As a part of an ongoing effort to develop new efficient anticancer organometallic drugs and to
81 palliate limitations in drug resistances and/or side effects, the synthesis of a novel copper(II) complex
82 of indenoisoquinoline ligand, named WN197, is established based on previous studies [54,55]. This

83   organo-copper complex effects were investigated on breast triple-negative MDA-MB-231, cervix
84   HeLa, and colon HT29 cell lines representative of three most prevalent adenocarcinomas, and
85   associated with poor prognostics. WN197 exerts a specific cytotoxic effect at low concentration (IC_{50}
86   below 0.5 µM) on the three cell lines and significantly below the value of human non-tumorigenic
87   epithelial cell line MCF-10A (IC_{50} 1.08 µM). WN197 acts as a Top1 poison and displays DNA
88   intercalation properties. The action mechanism of WN197 is further deciphered to bring insights into
89   its efficiency. DNA damage is detected by the presence of a rapid increase in nuclear phosphorylated
90   H2AX (after 30 min of treatment with 0.5 µM) and the main DDR kinases are activated by
91   phosphorylations. Cell cycle arrest in the G2 phase is confirmed by the inhibitory phosphorylation of
92   Cdk1 on tyrosine 15, an accumulation of cyclin B, and the unphosphorylated form of histone H3.
93   Furthermore, the cell cycle is halted in G2 by inhibitory phosphorylation of Cdc25C on serine 216
94   associated with a binding to the 14.3.3 chaperon. Cancer cells halt in G2, die by autophagy detected
95   through an increase in Beclin-1, and a decrease in the LC3-I/LC3-II ratio and the p62 marker.
96   Moreover, the RAPTOR component in the mTORC1 complex is phosphorylated on serine 792, a
97   feature of autophagic-induced cell death.

98   **2   Materials and Methods**

99   **2.1   Chemical reagents and materials**

100   All commercial reagents and solvents were used without further purification. Cisplatin is
101   purchased from Alfa Aesar (Heysham, UK); rapamycin from Abcam (Cambridge, UK); doxorubicin,
102   nocodazole and DMSO from Sigma-Aldrich (Saint-Quentin-Fallavier, France). Stock solutions were
103   prepared in DMSO. Melting points were determined with a Barnstead Electrothermal (BI 9300)
104   capillary melting point apparatus and are uncorrected. Elemental analyses were performed with a
105   varioMICRO analyser. Thin layer chromatography (TLC) was carried out on aluminium-baked
106   (Macherey-Nagel GmbH, Düren, Germany) silica gel 60. Column chromatography was performed on
107   silica gel (230-400 mesh). The electronic absorption spectra were acquired on a UV-Vis double beam
108   spectrophotometer SPECORD® PLUS (Analytik Jena GmbH, Germany). The molar conductance
109   measurement was carried out using a CDRV 62 Tacussel electronic bridge, employing a calibrated 10^{-2} M KCl solution and 10^{-3} M solutions of compounds in DMSO. Purities of all tested compounds were
110
111   ≥95%, as estimated by HPLC analysis. High Resolution Mass Spectrum (HR-MS) was measured at
112   REALCAT (Université de Lille) on a Synapt G2Si (Waters) equipped with an ion mobility cell.

113   **2.2   WN197 copper(II) indenoisoquinoline complex synthesis**

114   WN170 was synthesized according to the literature procedure [56]. To a solution of WN170 (160
115   mg, 0.443 mmol) in dry methanol (8 mL) was added dropwise a solution of $CuCl_2$ (59 mg, 0.443 mmol)
116   in MeOH (7 mL). After stirring at room temperature for 10 h, the reaction mixture was filtered off to
117   yield an orange precipitate which was washed with MeOH and dried under vacuum (8 h at 100 °C).
118   Yield: 132 mg (70%). Decomposition at 194 °C. Anal. Calcd. for $C_{44}H_{54}Cl_2CuN_6O_8$ (%): C, 56.86; H,
119   5.86; N, 9.04: Found C, 56.76; H, 5.89; N, 9.22. FT-IR (neat) (v_{max}, cm^{-1}): 1650 (C=O), 1549 (C=C),
120   490 (Cu-N). UV-vis in DMSO-H_2O (19/01), λ/nm (ε/$M^{-1}cm^{-1}$): 625 (156), 463 (4500) (9800), 353
121   (17620), 350 (18100), 328 (16440). Λ_M (1 mM, DMSO) (S cm^2 mol^{-1}): 24. HRMS (ESI) m/z: calcd
122   for $[M]^+$ $C_{44}H_{46}ClCuN_6O_4$ 820.2565; Found 820.2332.The equations should be inserted in editable
123   format from the equation editor.

124   **2.3   Cell culture**

125   HeLa, MDA-MB-231, HT-29 and MCF-10A cell lines originate from ATCC (Manassas, VA,
126   USA), and were maintained at 37 °C in a humidified atmosphere with 5% CO_2 in DMEM medium
127   (Lonza, Basel, Switzerland) supplemented with 10% fetal bovine serum (Dutscher, Dernolsheim,
128   France), 1% Zell Shield (Dutscher, Bernolsheim, France) and 1% non-essentials amino-acids (Lonza,
129   Basel, Switzerland). MCF-10A were maintained in MEBM medium (Lonza, Basel, Switzerland)
130   supplemented with MEGM (Lonza, Basel, Switzerland). All cell lines culture media were added with
131   1% Zell Shield (Dutscher, Bernolsheim, France).

2.4   Cell viability assay

133   Cell viability was determined using CellTiter 96® AQ$_{ueous}$ One Solution Cell Proliferation Assay
134   (MTS, Promega, Charbonnières-les-Bains, France). 2.10^3 cells well were seeded in 96-well plate for
135   24 h before treatment with 0 to 100 µM of WN197, WN170 or cisplatin for 72 h. After a 2 h incubation
136   with 20 µL of CellTiter solution at 37 °C in 5% CO_2, the production of reduced MTS (3-(4,5-
137   dimethylthiazol-2-yl)-5-(3-carboxymethoxyphenyl)-2-(4-sulfophenyl)-2H-tetrazolium) in formazan
138   was measured at 490 nm (SPECTROstar Nano, BMG LABTECH, Ortenberg, Germany). IC$_{50}$ were
139   calculated using GraphPad Prism V6.0 software. Statistical differences between WN197 and WN170
140   were ascertained by a Student t-test (**p<0.01 and ****p<0.0001).

2.5   Immunofluorescence for nuclei *foci*

142   2.10^5 cells seeded on glass coverslips were treated with 0.5 µM of WN197 or WN170, 5 µM of
143   doxorubicin, 20 µM of cisplatin as positive controls, or 0.1% DMSO as a solvent control for 30 min or
144   24 h. Fixation was performed with 4% paraformaldehyde (Sigma-Aldrich, Saint-Quentin-Fallavier,
145   France) for 5 min and followed by permeabilization with 0.1% Triton in PBS (Sigma-Aldrich, Saint-
146   Quentin-Fallavier, France) for 10 min and saturation of unspecific sites with 1% BSA in PBS (Sigma)
147   for 1 h at room temperature. Anti-γH2AX mouse antibody (S139, 1:1000, Cell Signalling, by Ozyme,
148   Saint-Cyr-L'École, France) was incubated overnight at 4 °C, washed 3 times with 1% BSA/PBS. Cells
149   were incubated with secondary anti-mouse IgG (Alexa Fluor® 488, 1:2000, Thermo-Fisher Scientific
150   Biosciences GMBH, Villebon-sur-Yvette, France) for 1 h at room temperature in the dark, washed 3
151   times before nuclei were stained with DAPI (6-diamidino-2-phenylindole, 1 µg/mL, Molecular Probes,
152   by Thermo Fisher Scientific Biosciences GMBH, Villebon-sur-Yvette, France). Images were captured
153   under a Leica fluorescent microscope, and γH2AX *foci* were counted with ImageJ (Fiji Software,
154   v1.52i) on 30 cells from 3 independent experiments and quantified with GraphPad Prism V6.0
155   software. Statistical significances (mean ± SD) were performed by a two-way ANOVA followed by
156   Dunnett's multiple comparison test (**p<0,01; ***p<0,001; ****p<0,0001).

2.6   Electrophoresis and Western blot

158    $7.5.10^5$ cells were seeded for 24 h and treated with 0.5 µM of WN197 or WN170, 20 µM of
159   cisplatin, 5 µM of doxorubicin, or 0.1% DMSO (solvent control). After 24 h, they were lysed in RIPA
160   buffer (1% Triton X-100; 50 mM TRIS-HCl pH 4; NP40 2%; 0.4% Na-deoxycholate; 0.6% SDS; 150
161   mM NaCl; 150 mM EDTA; 50 mM NaF) supplemented with 1% of protease inhibitor cocktail (Sigma-
162   Aldrich, Saint-Quentin-Fallavier, France) and phosphatase inhibitors (Roche SAS by Merck,
163   Kenilworth, NJ, USA).

164   For cytochrome C analysis, $7.5.10^5$ cells were seeded for 24 h and treated for 3 h, 16 h, 24 h or
165   48 h with 0.5 µM of WN197, and for 24 h or 48 h with 5 µM of doxorubicin as positive control. Cells
166   were lysed in a glass grinder at 4°C in homogenization buffer (25 mM MOPS at pH 7.2, 60 mM
167   β−glycerophosphate, 15 mM para-nitrophenylphosphate, 15 mM EDTA, 15 mM MgCl2, 2 mM DTT,

168   1 mM sodium orthovanadate, 1 mM NaF, 1 mM phenylphosphate, 10 μg/mL leupeptin, 10 μg/mL
169   aprotinin, 10 μg /mL soybean trypsin inhibitor, 10 μM benzamidine).

170   Samples were centrifuged for 10 min at 12,000 G and protein concentration of supernatants were
171   determined using the Bradford assay (BioRad, Marnes-la-Coquette, France) at 595 nm (SPECTROstar
172   Nano, BMG LABTECH, Ortenberg, Germany). Proteins were denatured in 2X Laemmli buffer (65.8
173   mM TRIS-HCl pH 6.8; 26.3% glycerol; 2.1% SDS; 0.01% bromophenol blue; 4% β-mercaptoethanol,
174   BioRad, Marnes-la-Coquette, France) at 75 °C for 10 min. 15 μg of proteins were separated on 4-20%
175   SDS PAGE gels (mini protean TGX, BioRad, Marnes-la-Coquette, France), for 1 h at 200 V in
176   denaturing buffer (0.1% SDS; 0.3% TRIS base; 1.44% glycine). Proteins were transferred onto
177   nitrocellulose membrane (Amersham Hybond, Dutscher, Bernolsheim, France) by wet transfer (0.32%
178   TRIS; 1.8% glycine; 20% methanol, Sigma-Aldrich, Saint-Quentin-Fallavier, France), for 1 h at 100
179   V. Membranes were saturated with 5% low fat dry milk in TBS added with 0.05% Tween (Sigma-
180   Aldrich, Saint-Quentin-Fallavier, France), and incubated overnight at 4 °C with specific primary
181   antibodies : rabbit polyclonal antibodies were against ATM (Cell Signaling technology (CST, by
182   Ozyme, Saint-Cyr-L'École, France), 1/1000), ATR (CST, 1/750), phosphorylated ATR (S428, CST,
183   1/1000), Beclin-1 (CST, 1/800), Cdc25C (CST, 1/1500), phosphorylated Cdc25C (S216, CST, 1/1000),
184   phosphorylated Cdk1 (Y15, CST, 1/1500), phosphorylated Chk1 (S317, CST, 1/1000), phosphorylated
185   Chk2 (T68, CST, 1/1000), cleaved caspase 3 (CST, 1/1000), phosphorylated H2AX (S139, CST,
186   1/750), histone H3 (CST, 1/1000), phosphorylated H3 (S10, CST, 1/1000), phosphorylated p53 (S15,
187   CST, 1/1000), p53 (CST, 1/1000), p21 (CST, 1/1000), LC3 (CST, 1/50), mTOR (CST, 1/1200),
188   RAPTOR (CST, 1:1500), phosphorylated RAPTOR (S792, CST, 1/1000); mouse monoclonal
189   antibodies against phosphorylated ATM (S1981, Santa Cruz Biotechnology (SCB), Santa Cruz, CA,
190   USA, 1/200), Chk1 (SCB, 1/1000), Chk2 (SCB, 1/200), Cdk1 (CST, 1/1000), 14-3-3 (SCB, 1/1000),
191   cyclin B2 (CST, 1/1500), p62 (SCB, 1/100); goat polyclonal antibodies against β-actin (SCB, 1/1200);
192   and cocktail antibodies against cleaved PARP (Abcam, Cambridge, UK, cell cycle and apoptosis
193   cocktail, 1/1500). After three washes of 10 min in TBS-Tween, nitrocellulose membranes were
194   incubated 1 h with the appropriate horseradish peroxidase-labeled secondary antibodies: anti-rabbit or
195   anti-mouse antibodies (Invitrogen, by Thermo Fisher Scientific Biosciences GMBH, Villebon-sur-
196   Yvette, France, 1/30,000) or anti-goat antibodies (SCB, 1/30,000). Secondary antibodies were washed
197   in TBS-Tween three times for 10 min and the signals were revealed with a chemiluminescent assay
198   (ECL Select, GE Healthcare, Dutscher, Bernolsheim, France) on hyperfilms (Amersham hyperfilm
199   MP, Dutscher, Bernolsheim, France). β-actin or histone H3 were used as loading controls. Signals were
200   quantified with Image J (Fiji Software, v1.52i), and normalized to respective loading control. The
201   means of 3 independent experiments were calculated.

2.7   *in vitro* activities of human topoisomerases I and II

203   Topoisomerase activities were examined in assays based on the relaxation of a supercoiled DNA
204   into its relaxed form. Topoisomerase I (Top1) activity was performed using the drug screening kits
205   protocol (TopoGEN, Inc., Buena Vista, CO, USA). The reaction mixture was composed of supercoiled
206   pHOT1 DNA (250 ng), 10X TGS buffer (10 mM Tris-HCl pH 7.9, 1 mM EDTA), 5 units of Top1, a
207   variable amount of compound to be tested, and a final volume adjusted to 20 μL with H2O. WN197
208   was tested at concentrations ranging from 0.2 to 2 μM. Camptothecin (10 μM) was used as a positive
209   control (poison inhibitor of Top1 activity), etoposide (100 μM) as negative control (inhibitor of Top2
210   activity), and 1% DMSO alone as vehicle control. Relaxed pHOT1 DNA (100 ng) was used as
211   migration control. The addition of proteinase K (50 μg/mL) for 15 min at 37 °C allowed Top1
212   degradation to visualize the cleavage products (nicked DNA). Reaction products were separated by

213 electrophoresis in a 1% agarose gel containing ethidium bromide (0.5 µg/mL) for 1 h at 100 V in TAE
214 (Tris-Acetate-EDTA; pH 8.3) buffer.

215   Topoisomerase II Relaxation Assay Kit (Inspiralis, Inc., Norwich, UK) was used to measure
216 topoisomerase II (Top2) activity. The reaction mixture was composed of supercoiled pBR322 DNA (1
217 µg), 10X assay buffer (50 mM Tris-HCl (pH 7.5), 125 mM NaCl, 10 mM MgCl2, 5 mM DTT, 100
218 µg/mL albumin), 30 mM ATP, 5 units of Top2α or Top2β, variable amount of compound to be tested,
219 and a final volume adjusted with H2O to 30 µL. Etoposide (VP-16, 100 µM) was used as positive
220 control, and camptothecin (10 µM) as negative control. The mixtures were incubated at 37 ℃ for 30
221 min and the reactions stopped by the addition of 5 µL 10% SDS. Reaction products were separated by
222 electrophoresis in a 1% agarose gel for 1 h at 100 V in TAE buffer, and stained with ethidium bromide
223 (0.5 µg/mL) for 15 min. After destaining in water, the DNA migratory profiles were visualized under
224 UV light (ChemiDocTM XRS+, BioRad, Marnes-la-Coquette, France).

225 **2.8   Melting temperature measurement**

226   Melting temperatures were obtained as described [54,55]. 20 µM solutions of WN170 or WN197
227 were prepared in 1 mL of BPE buffer (2 mM NaH$_2$PO$_4$, 6 mM Na$_2$PO$_4$, 1 mM EDTA, pH 7.1) in the
228 presence or not of 20 µM DNA from calf thymus (42% GC bp, Merck, Kenilworth, NJ, USA).
229 Absorbances were measured at 260 nm (Uvikon 943 coupled to Neslab RTE111) every minute over
230 the range of 20 to 100 °C with an increment of 1°C per minute. All spectra were recorded from 230 to
231 500 nm. Tested compound results are referenced against the same DNA concentration in the same
232 buffer. The Tm values were obtained from the first derived plots.

233 **2.9   Ethidium bromide competition test**

234   Fluorescence titrations were determined as described [54,55]. Ethidium bromide/WN170 or
235 WN197 molar ratio of 12.6/10 at concentrations ranging from 0.05 to 10 µM were used in a BPE buffer
236 (pH 7.1). The excitation wavelength was set at 546 nm and the emission was monitored over the range
237 of 560 to 700 nm (SPEX Fluorolog). IC$_{50}$ values for ethidium bromide (EB) displacement were
238 calculated using a fitting function incorporated into GraphPad Prism 6.0 software. The apparent
239 binding constants were calculated using the equation $K_{app} = (1.26 \ (K_{app}(EB)/IC_{50})$ with $K_{app}(EB) = 10^7$
240 M^{-1} and IC$_{50}$ in µM.

241 **2.10   Flow cytometry**

242      $7.5.10^5$ cells plated for 24 h were treated with 0.5 µM WN197 or WN170, 20 µM of cisplatin (S
243 phase arrest control), 83 nM of nocodazole (M phase arrest control), or 0.1% DMSO (solvent control).
244 For the dose titration experiments, cells were treated for 24 h with increasing concentrations of WN197.
245 For kinetic experiments, cells were treated with 0.5 µM of WN197 or WN170 from 4 to 48 h. Cells
246 were detached using trypsin (Biowest, Nuaillé, France)**,** centrifuged at 1,000 G for 10 min, resuspended
247 in PBS, and fixed with 70% ethanol at -20 °C for 24 h, before they were centrifugated (1,000 G, 10
248 min), resuspended in PBS, and treated for 15 min at room temperature with RNase (200 µg/mL,
249 Sigma). Finally, incubation with propidium iodide (10 µL/mL, Molecular Probes, by Thermo Fisher
250 Scientific Biosciences GMBH, Villebon-sur-Yvette, France) at 4 °C for 30 min was performed before
251 flow cytometry (BD FACSCalibur, Becton Dickinson, Le Pont-de-Claix, France) analysis. For each
252 sample, 10,000 events (without cell doublets and cellular debris) were considered. The cell cycle
253 repartition was analysed with Graphpad Prism V6.0 software. Statistical significances (mean ± SD)
254 were determined by two-way ANOVA followed by Dunnett's multiple comparison test
255 (****p<0,0001).

256 **2.11 Immunoprecipitation**

257   Cell lysates were obtained as described in the Western blot section. Samples were pre-cleared
258 with protein A sepharose (20 µL of 50% beads/ 200 µL of cell lysate, Sigma-Aldrich, Saint-Quentin-
259 Fallavier, France) for 1 h at 4 °C under gentle rocking. After brief centrifugation, supernatants were
260 incubated with antibodies against 14.3.3 (Santa Cruz Biotechnology, Santa Cruz, CA, USA, 1/200),
261 Cdc25C (Thermo Fisher Scientific Biosciences GMBH, Villebon-sur-Yvette, France, 1/200) or mTOR
262 (CST, 1/200) at 4 °C for 1 h under rotation and followed by incubation with protein A sepharose (20
263 µL of 50% bead slurry, Sigma-Aldrich, Saint-Quentin-Fallavier, France) for 1 h at 4 °C under rotation.
264 Samples were rinsed 3 times with RIPA buffer. Pellets were collected by brief centrifugation,
265 resuspended in 2X Laemmli buffer, and heated at 100 °C for 10 min before SDS-PAGE and Western
266 blots were performed.

267 **3   Results**

268 **3.1   Organocopper synthesis**

269   The synthesis of WN197 is described in **Figure 1**. Indenoisoquinoline WN170 was first obtained
270 in a four-step reaction. Condensation of the benzo[d]indeno[1,2-b]pyran-5,11-dione with a primary
271 aminoalcohol was followed by tosylation of the alcohol function. The substitution of the tosyl group
272 by the protected ethylenediamine and the consecutive deprotection of the Boc group led to WN170 in
273 68% global yield. Complex WN197 was then synthesized by reacting methanolic solutions of
274 indenoisoquinoline derivative WN170 and $CuCl_2$. After purification, WN197 was obtained in 70%
275 yield.

276 **3.2   WN197 displays a cytotoxic activity on three adenocarcinoma cell lines at low doses**

277   Cells viability was assayed on the triple-negative breast cancer cells (MDA-MB-231), the cervix
278 cancer cells (HeLa), and the colorectal cancer cells (HT-29) (**Table 1**). IC_{50} obtained are respectively
279 0.144 µM, 0.22 µM, and 0.358 µM for WN197 below the cisplatin IC_{50} values ranging from 10 to 40
280 µM. The copper-free indenoisoquinoline ligand, WN170, affected cell viability at higher doses (0.875
281 µM for MDA-MB-231, 0.630 µM for HeLa, and 0.479 µM for HT-29 cells), showing that the presence
282 of the copper metal significantly enhances the anticancer effect of the indenoisoquinoline core for
283 MDA-MB-231 and HeLa cell lines. A significantly higher IC_{50} (1.080 µM) is obtained on MCF-10A
284 compared to the adenocarcinoma cell lines (**Table 2**).

285 **3.3   WN197 induces DNA damage**

286   To determine whether WN197 affects DNA integrity, detection of γH2AX DNA break marker
287 was performed by immunofluorescence. γH2AX *foci* were visualized in the nucleus at 0.5 µM of
288 WN197, a concentration close to the IC_{50} determined previously, in MDA-MB-231, HeLa, and HT-
289 29. After 24 h of treatment, the average number of γH2AX *foci* per cell were respectively 99, 98, and
290 70 for MDA-MB-231, HeLa, and HT-29 cells (**Figure 2A**). The number of γH2AX *foci* was close to
291 the result obtained for the Top2 inhibitor, doxorubicin, (average of 95 *foci* per cell), and higher than
292 the number of γH2AX *foci* triggered by an alkylating agent, cisplatin (average of 55 *foci* per cell).
293 WN197 induced more DNA damage than the indenoisoquinoline WN170 (average of 23 *foci* per cell).
294 Controls with DMSO solvent showed a low number of *foci* (average of 9 *foci* per cell for the 3
295 adenocarcinomas) compared to treated conditions (**Figure 2B**).

296   These results were further confirmed by Western blot analysis (**Figure 2C**). Untreated cells
297   showed a low γH2AX signal while a strong signal was observed after doxorubicin, cisplatin, and
298   WN197 treatments. As observed by immunofluorescence, the γH2AX signal is weaker in the WN170
299   condition compared to the WN197 condition, indicating that the WN197 compound induces more DNA
300   damage than WN170 at the same concentration (0.5 µM).

301   *Foci* were detected as soon as 30 min after treatment (**Figure 2D**). The number of γH2AX *foci*
302   was close to the result obtained at 24 h with an average of *foci* per cell of 84, and 87 for MDA-MB-
303   231, HeLa, and lower to 13 for HT-29 cells after WN197 treatment.

3.4   WN197 is a concentration-dependent topoisomerase inhibitor

305   To determine whether the Cu(II)-complex WN197 is a topoisomerase inhibitor, *in vitro* human
306   topoisomerase activity tests were realized. The topoisomerase I (Top1) test relies on the ability of Top1
307   to relax supercoiled DNA, and the absence of relaxed DNA implies inhibition of Top1 activity. In the
308   presence of Top1, supercoiled DNA showed a relaxed profile (**Figure 3A**). Camptothecin, a well-
309   known Top1 inhibitor, disturbed DNA relaxation in the reaction, and part of the DNA remained
310   supercoiled. Increasing doses of WN197 from 0.2 to 2 µM showed a decrease quantity of relaxed DNA,
311   indicating disruption of Top1 activity. The solvent control, DMSO, and VP-16 (etoposide, a Top2
312   inhibitor) displayed no effect on Top1-induced DNA relaxation showing no inhibitory effect on Top1
313   activity.

314   Top1 inhibitors can act either as catalytic inhibitors by DNA intercalation at the Top1 fixation
315   site or as poisons, forming a ternary complex (DNA + Top1 + compound) [24,25], preventing DNA
316   religation and inducing accumulation of nicked DNA. The addition of proteinase K to the Top1-DNA
317   relaxation test allows the release of nicked DNA that can be resolved and detected on agarose gel. The
318   short half-life of the nicked DNA is stabilized and detectable after addition of a Top1 poison,
319   camptothecin (**Figure 3A**). Nicked DNA was also observed in presence of 0.2 µM of WN197,
320   indicating a Top1 poison activity (**Figure 3A**). At higher concentrations (0.5 µM, 1 µM, 2 µM), the
321   inhibition of Top1 activity without nicked DNA accumulation indicates that WN197 does not act as a
322   Top1 poison.

323   The effect of WN197 on Top2α and Top2β activities were also assayed. The same principle based
324   on the inhibition of topoisomerase-induced DNA relaxation was used (**Figure 3B**). In the presence of
325   Top2α or Top2β, the supercoiled DNA is relaxed (topoisomers). VP-16 (etoposide, Top2 inhibitor)
326   disturbed DNA relaxation in the reaction, as seen by the presence of supercoiled DNA in the gel, while
327   camptothecin had no inhibitory effect, as expected. WN197 disrupted the Top2α-induced DNA
328   relaxation only at 2 µM, and the Top2β at 1 and 2 µM, higher doses than the concentration necessary
329   to inhibit Top1 activity, indicating a concentration-dependent mechanism of action.

3.5   WN197 intercalates in DNA

331   Melting curves and fluorescence measurements were performed to comfort results obtained in
332   **figure 3**, and ascertain WN197 intercalation in DNA.

333   Drugs ability to protect calf thymus DNA (CT DNA, 42% GC bp) against thermal denaturation
334   was used as an indicator of the capacity of indenoisoquinoline derivatives to bind and stabilize the
335   DNA double helix. The Cu(II) indenoisoquinoline complex WN197 displayed a slightly higher ΔTm
336   value compared to the metal-free indenoisoquinoline WN170 (respectively 16.6 °C and 16.1 °C,
337   drug/DNA ratio 0.5), showing a better binding affinity with DNA (**Table 3**).

338   The binding affinities, determined using a fluorescence quenching assay based on DNA binding
339   competition between the intercalating drug ethidium bromide and the tested molecules, were used to
340   gain insight into the DNA binding affinity. The apparent DNA binding constant Kapp value of the
341   Cu(II) complex ($15.005\pm0.290\ 10^7\ M^{-1}$) is higher compared to the original ligand value (2.436 ± 0.883
342    $10^7\ M^{-1}$). These results are in agreement with the ΔTm values showing that the complexation of
343   indenoisoquinoline ligand by copper allows a stronger interaction with DNA (**Table 3**).

344   **3.6   WN197 activates the DNA Damage Response pathway**

345   The activation of molecular effectors of the DDR pathways involved in SSB and DSB was
346   analysed by Western blot (**Figure 4**). Activating phosphorylation of ATR (S428) and ATM (S1981)
347   occurred in the three cell lines MDA-MB-231, HeLa, and HT-29 treated with WN197 compared to the
348   untreated cells. The subsequent activating phosphorylation of Chk1 (S317) and Chk2 (T68) were
349   observed, confirming the DDR pathway activation. In the doxorubicin, cisplatin, and WN170 these
350   phosphorylations also occurred while in untreated controls they were always lower or absent.

351   p53 facilitates cell cycle arrest by targeting p21$^{WAF1/CIP1}$. After WN197 treatment, p53 and
352   phosphorylated p53 were increased in MDA-MB-231, HeLa and HT-29 cells (respectively by factors
353   34.8, 3.2, and 1.6 for p53 and by 58.3, 1.6 and 5.5 for phosphorylated p53), while p21 was highly
354   increased in HT-29 cells (by a factor 8.3) compared to MDA-MB-231 and HeLa (respectively 1.3 and
355   2.2). The WN170 values are slightly identical except for p53 and p21 in MDA-MB-231 (respectively
356   factors 0.4 and 1.0). In doxorubicin and cisplatin treated cell lines, p53 and p21 were not increased
357   except for p53 in MDA-MB-231 and p21 in HT-29 cells.

358   **3.7   WN197 induces a cell cycle arrest in G2 phase**

359   The cell cycle repartition following the DDR pathway activation was monitored by flow
360   cytometry in cells exposed for 24 h to different treatments (**Figure 5A**). Untreated cells showed a
361   classical cell cycle repartition in the 3 cell lines with averages of 50.52% cells in G0/G1 phases, 29.80%
362   in the S phase and 19.68% in the G2/M phases. Cisplatin, known to promote the accumulation of cells
363   in the S phase [57,58], induced 79.79%, 59.61%, and 85.53% cells in S phase for MDA-MB-231,
364   HeLa, and HT-29 cells, respectively. The mitotic spindle poison, nocodazole, led to an arrest in mitosis
365   with 70.17%, 88.61%, and 39.68% cells in G2/M phase for MDA-MB-231, HeLa, and HT-29,
366   respectively. WN170 did not modified the cell cycle repartition of MDA-MB-231 cells and induced a
367   G2/M accumulation of HeLa and HT-29 cell lines. Treatments with WN197 triggered a G2/M phase
368   accumulation. WN197 had the capacity to induce a higher percentage of cells accumulation in the
369   G2/M phase compared to WN170 respectively with 51.29% and 21.08% for MDA-MB-231 cells,
370   70.51% and 54.19% for HeLa cells, and 74.4% and 48.06% for HT-29 cells. Sub-G1 peaks were not
371   observed in WN197 treated cells, while they were present after doxorubicin treatment (positive
372   apoptotic control) in supplementary **Figure S1**.

373   To determine the lower dose necessary to induce a G2/M phase accumulation, flow cytometry
374   experiments were performed with increasing concentrations of WN197 and results are shown in **Figure
375   5B**. A G2/M phase accumulation was significantly induced by WN197 from 0.5 to 1 µM for MDA-
376   MB-231, 0.25 to 0.5 µM for HeLa and 0.25 to 1 µM for HT-29.

377   A kinetic of treatment with WN197 (0.5 µM) was realized on the three adenocarcinoma cell lines
378   by flow cytometry to determine the earliest-induced G2/M accumulation (**Figure 5C**). After 8 h of
379   treatments, the cell cycle was modified for MDA-MB-231 with a significant accumulation in G2/M. A
380   later effect after 12 h and 16 h of treatment was observed respectively for HT-29 and HeLa.

381   Cell cycle arrest phase was further determined by Western blot analysis of major cell cycle
382 regulators: Cdk1, cyclin B, Cdc25C phosphatase, and histone H3. (**Figure 6A**). The Cdk1/cyclin B
383 complex that forms the also called MPF (M-phase Promoting Factor) is required for the transition from
384 G2 to M phase of the cell cycle. During the G2/M transition, Cdk1 is activated by dephosphorylation
385 of its threonine 14 and tyrosine 15 residues (inhibitory phosphorylations) by the active Cdc25C
386 phosphatase that requires prerequisite dephosphorylation on threonine 161 [59,60]. In comparison to
387 the untreated control, the phosphorylation of Cdk1 on tyrosine 15 was increased after cisplatin, WN170
388 or WN197 treatments in the three adenocarcinoma cell lines, while it decreased after treatments with
389 doxorubicin or nocodazole in HeLa and HT-29 and was slightly identical in MDA-MB-231 treated
390 with doxorubicin. The cyclin B amount was increased after WN197 treatment in the three cell lines.
391 Cdc25C was decreased in MDA-MB-231 and HT-29, and increased in HeLa after treatments with
392 WN197 compared to untreated conditions. The inhibitory phosphorylation of Cdc25C on serine 216
393 was enhanced by WN197 treatments compared to untreated conditions in the three cell lines. On the
394 contrary, a decrease of this phosphorylation was obtained after nocodazole treatments, consistent with
395 the former detection of an activated form of MPF except for HT-29. Finally, histone H3
396 phosphorylation on serine 10 is involved in mitotic chromatin condensation and is a marker for entry
397 in the M phase after activation of the Cdk1/Cyclin B complex [61]. In WN197 treated cells, histone
398 H3 was not phosphorylated on serine 10, showing that cancer cells were stopped in the G2 phase before
399 they could reach the M phase. On the contrary in nocodazole treated adenocarcinoma lines in which
400 an arrest in the M phase occurs, histone H3 was phosphorylated on serine 10.

401   Furthermore, as seen in **Figure 6B**, Cdc25C phosphorylated on serine 216 was trapped by 14-3-
402 3 as shown by Cdc25C or 14-3-3 immunoprecipitations realized in HeLa, and Cdc25C
403 immunoprecipitations in MDA-MB-231 and HT-29 cells after 24 h of treatment with 0.5 µM of
404 WN197. The binding was observed after cisplatin treatment but not in untreated controls.

405 **3.8   WN197 induces autophagy**

406   Apoptosis is often activated after DNA damage [25,62]. However, the early apoptosis marker
407 cleaved caspase 3 and the late apoptosis marker cleaved PARP were not detected after treatments with
408 WN197 and WN170 in contrast to doxorubicin and cisplatin treatments (**Figure 7A**). A time-course
409 detection of cleaved PARP and cytochrome C release in the cytoplasm at 3, 16, 24, 48, and 72 h
410 compared to doxorubicin apoptosis positive control at 24 and 48 h (**Figure 7B and 7C**) and annexin
411 V tests (**Figure S2**) confirm apoptosis is not triggered by WN197. These data indicate that apoptosis
412 is not the programmed cell death activated.

413   We then determined whether WN197 and WN170 could induce autophagy. In the three
414 adenocarcinoma cell lines, several autophagy markers [63] were detected. p62/sequestosome-1 was
415 degraded, Beclin-1 was synthesized and LC3-I association with phosphatidyl-ethanolamine that forms
416 LC3-II was increased as shown by accumulation of LC3-II after 24h of treatment with 0.5 µM of
417 WN197 and WN170 (**Figure 7D**). The same changes were observed with the inhibitor of mTOR
418 pathway, rapamycin which is known to activate the autophagy process. Moreover,
419 immunoprecipitation carried on the mTOR complex showed that the RAPTOR component was
420 phosphorylated on serine 792 after treatment with 0.5 µM of WN197, as seen in positive controls
421 treated with 500 nM of rapamycin, and compared to negative controls treated with doxorubicin (**Figure
422 7E**).

423 **4   Discussion**

424   This study aims to develop and understand the molecular properties of a new organometallic
425   compound WN197, derived from the topoisomerase 1 inhibitor indenoisoquinoline. Previous studies
426   highlighted action specifically correlated to the presence of a metallic atom like copper [53], iron (e.g.
427   ferrocen/ferroquine [43,64]), ruthenium (e.g. indenoisoquinoline [55] and various complexes [65,66]),
428   or platin (e.g. cisplatin [67]), and demonstrate the interest of these organometallic compounds in
429   cancerology. More recently, a class of topoisomerase inhibitor, the indenoisoquinoline derivatives,
430   were developed and selected for their high stability and non-drug substrate for efflux transporters
431   involved in cell resistance [35,68]. These promising compounds are in phase I/II clinical trials [36,68].
432   However, constant efforts are made to increase their efficiency. The addition of a carbohydrate moiety
433   to indenoisoquinoline derivatives significantly improves the binding affinity to DNA due to a stronger
434   interaction through hydrogen bonds [69]. Hereby, we synthesised a new copper indenoisoquinoline
435   derivative. The copper(II) addition to the indenoisoquinoline backbone significantly enhance the
436   toxicity on triple-negative breast MDA-MB-231 and cervix HeLa cancer cell lines. Those two cell lines
437   are related to breast and cervix cancers with high mortality rates in women. In addition, the toxicity is
438   obtained at lower doses compared to human non-tumorigenic epithelial cell line MCF-10A. The use of
439   low doses in chemotherapy could be of particular interest and represent an advantage with less risk of
440   adverse side effects. Further experiments will help to determine if WN197 has specificity at the cellular
441   level.

442   The viability assays showed that low doses are necessary to induce cell death in breast, cervix,
443   and colon cancer cell lines, from three of the most prevalent adenocarcinomas. The IC_{50} are under the
444   values obtained for most other Top1 inhibitors that usually range from concentration of 1 to 10 μM
445   except for thiosemicarbazone or pyrimidine-derived compounds [53]. The medium value of 0.5 μM,
446   close to the IC_{50} for the three adenocarcinoma cell lines, was further chosen to decipher the molecular
447   pathways involved in the anti-proliferative effect of WN197. Topoisomerases are overexpressed in M
448   phase in cancer cells and generate a high number of DNA breaks under the action of Top inhibitors
449   [12,14,15]. Cells overexpressing topoisomerases have shown better responses to Top inhibitors
450   [70,71]. Using low doses of the compound could be useful to avoid unwanted normal cell death. Such
451   strategies of low minimal but necessary anti-tumorigenic doses are often employed for anthracycline
452   to limit cardiotoxicity [72,73].

453   We determined the extent of DNA damage induced by the new compound, with
454   immunofluorescence and Western blot analysis of a front-line activated marker of DNA breaks, the
455   γH2AX histone. The recruitment of γH2AX normally occurs at the site of DNA breaks after exposition
456   to Top1 or Top2 poisons [74,75]. Higher level of DNA breaks is observed with WN197 compared to
457   the control copper-free compound WN170, proving that the presence of a metal atom increases the
458   efficiency to induce DNA damage. DNA breaks appear early around 30 min after addition of the
459   product. In parallel, *in vitro* tests reveal that WN197 inhibits Top1 at low doses, corresponding to the
460   IC_{50}, and Top2 at higher doses up to 1 μM showing a dose-dependent action. The copper complex
461   WN197 is a Top1 poison that forms a ternary complex with the DNA (interfacial inhibition) as
462   indenoisoquinoline derivatives [24].

463   After DNA damage is induced, DDR effectors are activated, as shown in Western blot
464   experiments. The upstream kinases ATM, ATR, Chk1, and Chk2 are phosphorylated after 24 h of
465   treatment with 0.5 μM of WN197, a prerequisite for their activation [76,77]. Both SSB (ATR, Chk1)
466   and DSB (ATM, Chk2) markers are detected at a concentration capable to inhibit Top1. Top1 are
467   known to generate SSB and Top2 DSB. However, Top1 poisons produce SSB that can be converted
468   into DSB, the most dangerous type of DNA break, at the replication fork stalling [78,79] explaining
469   the activation of both SSB and DSB markers in our experiments. The cell cycle arrest induced by 0.5

470 µM of WN197 occurs in the G2/M phase for all cancer cell lines analysed, as early as 8 h or 16 h with
471 a maximal number of arrested cells after 24 h of treatment and is maintained at 48 h. Concentration
472 values ranging from 0.25 µM to 1 µM of WN197 are necessary to trigger the G2/M arrest. This result
473 is consistent with the dose-dependent inhibitory effect obtained in the *in vitro* topoisomerase inhibition
474 tests where Top1 inhibition is obtained with values between 0.2 µM and 0.5 µM. Above 1 µM a
475 different DNA migration profile is detected showing WN197 poison activity is lost for a different type
476 of inhibition. A catalytic mode of inhibition could occur through intercalation of WN197 into DNA.
477 At doses above 1 µM, the compound exerts a dual Top1/Top2 inhibitory activity and intercalation
478 properties as demonstrated by the melting curves and the fluorescence measurements. The planar
479 indenoisoquinoline skeleton of WN197 displays an increased intercalation into DNA compared to
480 WN170. The high affinity of the Cu(II) complex with DNA can be attributed to the π-cation interaction
481 between the base pairs and the atom of Cu(II) coordinated with ligands, but also to the capability to
482 increase the π-π interaction between the base pairs of DNA and a second ligand molecule [80,81]. At
483 high doses, DNA intercalation could avoid topoisomerase access to its fixation site similarly to a
484 catalytic inhibitor. Such mechanism is found with anthracyclines such as doxorubicin whose poison
485 activity at low doses is lost for an intercalating catalytic inhibitory activity at high doses. Due to a
486 strong affinity for DNA duplexes, those anthracycline compounds prevent Top2 binding to DNA
487 [75,82].

488 To determine the exact arrest phase in the cell cycle, analyses were further conducted. To allow
489 the G2 to M phase transition, Cdc25C dephosphorylates on residues tyrosine 15 and threonine 14,
490 leading to its activation [83,84]. Cdk1 activation in the MPF complex phosphorylates histone H3 on
491 serine 10 to allow DNA condensation during mitosis [61]. After 24 h of treatments, an increase in the
492 inhibitory serine 216 phosphorylation of Cdc25C is detected. This phosphorylation is recognized by
493 14-3-3 [85] to form a complex with Cdc25C, as shown in the three adenocarcinomas, by
494 immunoprecipitation. Sequestration of Cdc25C by 14.3.3 impedes Cdk1 dephosphorylation on tyrosine
495 15 and histone H3 phosphorylation does not occur on serine 10 in the three cell lines after treatment
496 with WN197 for 24 h. The cancer cell lines lack the required MPF activation and H3 phosphorylation
497 to allow an M phase entry and remain arrested in G2. In addition, cyclin B accumulates in our
498 experiments concomitantly and is not destroyed by the proteasome as expected at the end of the M
499 phase [86,87]. p53 and its target the cell cycle inhibitor p21 are increased after WN197 treatments. p53
500 is involved in cell-cycle arrest by a transcriptional activation of p21 capable to inhibit Cdk1/cyclin B
501 and cell-cycle progression through mitosis [88–90]. p53 also targets 14-3-3 and blocks G2/M transition
502 [91]. Altogether, the results demonstrate that WN197 at low doses with a Top1 poison activity arrest
503 adenocarcinoma cells in G2. After DNA damage have been induced, activation of the DDR pathways
504 normally ensures repairs but when damage is too extended, cells undergo a programmed death [92,93].
505 While most of the actual topoisomerase inhibitors induce apoptosis [25,62], WN197 triggers
506 autophagy. Among topoisomerase I inhibitors, a camptothecin derivative irinotecan and an
507 indenoisoquinoline compound NSC706744 were reported to activate autophagy with the absence of
508 apoptosis [94, 95]. After 24 h of treatment with low doses of WN197 (0.5 µM), autophagy markers are
509 detected by Western blots: synthesis of Beclin-1 [96], increase in LC3-II/LC3-I ratio [97], and
510 degradation of p62 [98]. It was previously shown, after DNA damage, that the mTORC1 complex was
511 inhibited by RAPTOR phosphorylation (on multiple sites including serine 792) in a negative feedback
512 loop to induce autophagy [99, 100]. We further show autophagy is triggered through the
513 phosphorylation of RAPTOR in the mTOR complex. This mechanism of activation is similar to the
514 mTORC1 inhibitor rapamycin [101]. Our results show that under WN197 treatment from 3 to 72 h,
515 cells die by a caspase-independent mechanism as classical markers annexin V staining, caspase 3 and
516 PARP cleavage, cytoplasmic cytochrome C released were not detected. It also has to be noted, no sub-
517 G1 cells were detected after WN197 treatment while they were after doxorubicin known to induce

518 apoptosis. Previous data on breast cancer cells have showed autophagy could mask and delay apoptosis
519 but was associated with an early release of cytochrome C from mitochondria which is not the case in
520 our experiments [102]. Cytochrome C is not released when autophagy is triggered and mitochondria
521 degraded in autophagosomes [103]. Several studies have described autophagy as dependent on wild-
522 type p53 depletion or inhibition [104]. WN197 action is associated with an increase in p53 and p53
523 phosphorylation. However, the induced-autophagy does not dependent on the cell lines p53 status.
524 HeLa cells express wild-type p53 that end up as functionally null when targeted to degradation by E6
525 endogenous papillomavirus protein, while MDA-MB-231 and HT-29 display p53 mutations resulting
526 in positive gain of function [105]. Nevertheless, WN197 induced-autophagy is in agreement with an
527 increase of p21 level and the G2 arrest detected our experiments in cancer cells. Several anti-apoptotic
528 effects of p21 can explain the choice of an autophagic cell death instead of apoptosis. High levels of
529 p21 are known to block Cdk1/cyclin B and to inhibit apoptosis through down-regulation of caspase-2
530 [106], stabilization of anti-apoptotic cellular inhibitor of apoptosis protein-1, c-IAP1 [107], and
531 inhibition of procaspase 3 activity [108]. Another additional mechanism through Beclin-1 could play
532 an important role in apoptosis inhibition and autophagy. Beclin-1 protein expression was shown
533 necessary to block the apoptotic cascade after induced-DNA damage [102, 109] and to activate
534 autophagy under low doses of chemotherapeutics (rapamycin, tamoxifen) in breast and ovarian cancers
535 [110, 111].

536 **5 Conclusion**

537 Copper(II) indenoisoquinoline complex WN197 displays an anti-cancerous activity at low doses
538 inhibiting Top1. MDA-MB-231 (triple negative breast cancer cells), HeLa (cervix cancer cells), and
539 HT-29 (colon cancer cells), cancer cells accumulate DNA breaks and arrest in the G2 phase of the cell
540 cycle. This arrest is characterized by the inactivation of the Cdc25C phosphatase through
541 phosphorylation on serine 216 and binding to 14.3.3 that consequently leaves in its inactive form the
542 MPF (a phosphorylated form of Cdk1 associated to accumulated cyclin B). Autophagy is further
543 processed by the RAPTOR effector phosphorylation in the mTOR complex, and associated to p21
544 overexpression. WN197 appears as a new efficient drug to counteract cancer cells when used at low
545 doses. The action mechanism of the copper complex is summarized in figure 8. Its use in chemotherapy
546 could particularly benefit patients with cancer cells overexpressing topoisomerases or sensitize cancer
547 cells to other DNA modifying agents including DNA adducts inducer, methylating agents, or PARP
548 inhibitors [112, 113].

549 **5   Conflict of Interest**

552 **6   Author Contributions**

555 **7   Funding**

8 Acknowledgments

9 Data Availability Statement

The data that support the findings of this study are included in this manuscript.

10 Abbreviations

ATM, ataxia telangiectasia mutated; ATR, ataxia telangiectasia related; BSA, bovine serum albumin; Cdc25, cell division cycle 25; Cdk1, cyclin dependent kinase 1; Chk1/2, checkpoint kinases 1/2; c-IAP1, cellular inhibitor of apoptosis protein 1; DDR, DNA damage response; DNA-PK, DNA-dependent protein kinase; DSB, double strand break; H2AX, H2A histone family member X; IC_{50}, half maximal inhibitory concentration; Kapp, apparent dissociation constant; mTOR, mammalian target of rapamycin; MTS, 3-(4,5-dimethylthiazol-2-yl)-5-(3-carboxymethoxyphenyl)-2-(4-sulfophenyl)-2H-tetrazolium; $_N$DNA, nicked DNA; PBS, phosphate-buffered saline; RAPTOR, regulatory-associated protein of mTOR; $_R$DNA, relaxed DNA; $_{SC}$DNA, supercoiled DNA; SDS, sodium dodecyl sulfate; SSB, single strand break; t-AML, therapy-related acute myeloid leukemia; TLC, thin-layer chromatography; Tm, temperature of melting; Top, Topoisomerase; VP-16, etoposide.

11 References

1 Bray F, Ferlay J, Soerjomataram I, Siegel RL, Torre LA & Jemal A (2018) Global cancer statistics 2018: GLOBOCAN estimates of incidence and mortality worldwide for 36 cancers in 185 countries. *CA Cancer J Clin* **68**, 394–424. doi: 10.3322/caac.21492

2 Curtin NJ (2012) DNA repair dysregulation from cancer driver to therapeutic target. *Nat Rev Cancer* **12**, 801–817. doi: 10.1038/nrc3399

3 O'Connor MJ (2015) Targeting the DNA Damage Response in Cancer. *Mol Cell* **60**, 547–560. doi: 10.1016/j.molcel.2015.10.040

4 Fernández X, Díaz-Ingelmo O, Martínez-García B & Roca J (2014) Chromatin regulates DNA torsional energy via topoisomerase II-mediated relaxation of positive supercoils. *EMBO J* **33**, 1492–1501. doi: 10.15252/embj.201488091

5 Pommier Y, Sun Y, Huang SYN & Nitiss JL (2016) Roles of eukaryotic topoisomerases in transcription, replication and genomic stability. *Nat Rev Mol Cell Biol* **17**, 703–721. doi: 10.1038/nrm.2016.111

6 Nielsen CF, Zhang T, Barisic M, Kalitsis P & Hudson DF (2020) Topoisomerase IIa is essential for maintenance of mitotic chromosome structure. *Proc Natl Acad Sci U S A* **117**. doi: 10.1073/pnas.2001760117

7 Hanke A, Ziraldo R & Levene SD (2021) DNA-topology simplification by topoisomerases. *Molecules* **26**, 1–24. doi: 10.3390/molecules26113375

8 Spakman D, Bakx JAM, Biebricher AS, Peterman EJG, Wuite GJL & King GA (2021) Unravelling the

596 mechanisms of Type 1A topoisomerases using single-molecule approaches. *Nucleic Acids Res* **49**, 5470–
597 5492. doi: 10.1093/nar/gkab239

598 9 Pommier Y, Leo E, Zhang H & Marchand C (2010) DNA topoisomerases and their poisoning by anticancer
599 and antibacterial drugs. *Chem Biol* **17**, 421–433. doi: 10.1016/j.chembiol.2010.04.012

600 10 Branca M, Giorgi C, Ciotti M, Santini D, Di Bonito L, Costa S, Benedetto A, Bonifacio D, Di Dibonito P,
601 Paba P, Accardi L, Mariani L, Ruutu M, Syrjänen SM, Favalli C & Syrjänen K (2006) Over-expression of
602 topoisomerase IIα is related to the grade of cervical intraepithelial neoplasia (CIN) and high-risk human
603 papillomavirus (HPV), but does not predict prognosis in cervical cancer or HPV clearance after cone
604 treatment. *Int J Gynecol Pathol* **25**, 383–392. doi: 10.1097/01.pgp.0000209573.54457.32

605 11 Coss A, Tosetto M, Fox EJ, Sapetto-Rebow B, Gorman S, Kennedy BN, Lloyd AT, Hyland JM, O'Donoghue
606 DP, Sheahan K, Leahy DT, Mulcahy HE & O'Sullivan JN (2009) Increased topoisomerase IIα expression
607 in colorectal cancer is associated with advanced disease and chemotherapeutic resistance via inhibition of
608 apoptosis. *Cancer Lett* **276**, 228–238. doi: 10.1016/j.canlet.2008.11.018

609 12 Heestand GM, Schwaederle M, Gatalica Z, Arguello D & Kurzrock R (2017) Topoisomerase expression and
610 amplification in solid tumours: Analysis of 24,262 patients. *Eur J Cancer* **83**, 80–87. doi:
611 10.1016/j.ejca.2017.06.019

612 13 Shigematsu H, Ozaki S, Yasui D, Yamamoto H, Zaitsu J, Taniyama D, Saitou A, Kuraoka K, Hirata T &
613 Taniyama K (2018) Overexpression of topoisomerase II alpha protein is a factor for poor prognosis in
614 patients with luminal B breast cancer. *Oncotarget* **9**, 26701–26710. doi: 10.18632/oncotarget.25468

615 14 Villman K, Ståhl E, Liljegren G, Tidefelt U & Karlsson MG (2002) Topoisomerase II-α expression in
616 different cell cycle phases in fresh human breast carcinomas. *Mod Pathol* **15**, 486–491. doi:
617 10.1038/modpathol.3880552

618 15 Lee YC, Lee CH, Tsai HP, An HW, Lee CM, Wu JC, Chen CS, Huang SH, Hwang J, Cheng KT, Leiw PL,
619 Chen CL & Lin CM (2015) Targeting of Topoisomerase I for Prognoses and Therapeutics of
620 Camptothecin-Resistant Ovarian Cancer. *PLoS One* **10**, 1–19. doi: 10.1371/journal.pone.0132579

621 16 Cortez D (2019) Replication-Coupled DNA Repair. *Mol Cell* **74**, 866–876. doi:
622 10.1016/j.molcel.2019.04.027

623 17 Toledo L, Neelsen KJ & Lukas J (2017) Replication Catastrophe: When a Checkpoint Fails because of
624 Exhaustion. *Mol Cell* **66**, 735–749. doi: 10.1016/j.molcel.2017.05.001

625 18 Gan W, Guan Z, Liu J, Gui T, Shen K, Manley JL & Li X (2011) R-loop-mediated genomic instability is
626 caused by impairment of replication fork progression. *Genes Dev* **25**, 2041–2056. doi:
627 10.1101/gad.17010011

628 19 Surova O & Zhivotovsky B (2013) Various modes of cell death induced by DNA damage. *Oncogene* **32**,
629 3789–3797. doi: 10.1038/onc.2012.556

630 20 Roos WP & Kaina B (2013) DNA damage-induced cell death: From specific DNA lesions to the DNA
631 damage response and apoptosis. *Cancer Lett* **332**, 237–248. doi: 10.1016/j.canlet.2012.01.007

632 21 Sharma A, Singh K & Almasan A (2012) Histone H2AX phosphorylation: A marker for DNA damage.
633 *Methods Mol Biol* **920**, 613–626. doi: 10.1007/978-1-61779-998-3_40

634   22 Smith HL, Southgate H, Tweddle DA & Curtin NJ (2020) DNA damage checkpoint kinases in cancer. *Expert*
635   *Rev Mol Med* **8,** e2. doi: 10.1017/erm.2020.3

636   23 Liu K, Zheng M, Lu R, Du J, Zhao Q, Li Z, Li Y & Zhang S (2020) The role of CDC25C in cell cycle
637   regulation and clinical cancer therapy: A systematic review. *Cancer Cell Int* **20**, 1–16. doi:
638   10.1186/s12935-020-01304-w

639   24 Pommier Y, Kiselev E & Marchand C (2015) Interfacial inhibitors. *Bioorganic Med Chem Lett* **25**, 3961–
640   3965. doi: 10.1016/j.bmcl.2015.07.032

641   25 Larsen AK, Escargueil AE & Skladanowski A (2003) From DNA damage to G2 arrest: the many roles of
642   topoisomerase II. *Prog Cell Cycle Res* **5**, 295–300. PMID: 14593724

643   26 Eikenberry S (2009) A tumor cord model for Doxorubicin delivery and dose optimization in solid tumors.
644   *Theor Biol Med Model* **6**, 1–20. doi: 10.1186/1742-4682-6-16

645   27 Conte PF, Gennari A, Landucci E & Orlandini C (2000) Role of epirubicin in advanced breast cancer. *Clin*
646   *Breast Cancer* 1 Suppl 1, S46–S51. doi: 10.3816/cbc.2000.s.009

647   28 Al. MP at (2015) Topoisomerase II and leukemia MaryJean. *Ann N Y Acad Sci* **1310**, 98–110. doi:
648   10.1111/nyas.12358

649   29 Kalyanaraman B (2020) Teaching the basics of the mechanism of doxorubicin-induced cardiotoxicity: Have
650   we been barking up the wrong tree? *Redox Biol* **29**, 101394. doi: 10.1016/j.redox.2019.101394

651   30 Zhang W, Gou P, Dupret JM, Chomienne C, Rodrigues-Lima F. (2021) Etoposide, an anticancer drug
652   involved in therapy-related secondary leukemia: Enzymes at play. *Transl Oncol.* **10**, 101169. doi:
653   10.1016/j.tranon.2021.101169

654   31 Cappetta D, De Angelis A, Sapio L, Prezioso L, Illiano M, Quaini F, Rossi F, Berrino L, Naviglio S &
655   Urbanek K (2017) Oxidative stress and cellular response to doxorubicin: A common factor in the complex
656   milieu of anthracycline cardiotoxicity. *Oxid Med Cell Longev* **2017**. doi: 10.1155/2017/1521020

657   32 Sritharan S & Sivalingam N (2021) A comprehensive review on time-tested anticancer drug doxorubicin.
658   *Life Sci* **278**, 119527. doi: 10.1016/j.lfs.2021.119527

659   33 Li F, Jiang T, Li Q & Ling X (2017) Camptothecin analogues and their molecular targets. *Am J Cancer Res*
660   **7**, 2350–2394. PMID: 29312794

661   34 Holcombe RF, Kong KM & Wimmer D (2004) Combined topoisomerase I inhibition for the treatment of
662   metastatic colon cancer. *Anticancer Drugs* **15**, 569–574. doi: 10.1097/01.cad.0000132232.28888.21

663   35 Pommier Y, Cushman M & Doroshow JH (2018) Novel clinical indenoisoquinoline topoisomerase I
664   inhibitors: A twist around the camptothecins. *Oncotarget* **9**, 37286–37288. doi:
665   10.18632/oncotarget.26466

666   36 Thomas A & Pommier Y (2019) Targeting topoisomerase I in the era of precision medicine. *Clin Cancer Res*
667   **25**, 6581–6589. doi: 10.1158/1078-0432.CCR-19-1089

668   37 Rosenberg B, VanCamp L, Trosko JE, Mansour VH. (1969) Platinum compounds: a new class of potent
669   antitumour agents. *Nature.* **5191**, 385-386. doi: 10.1038/222385a0

670   38 Alderden RA, Hall MD & Hambley TW (2006) The discovery and development of cisplatin. *J Chem Educ*
671   **83**, 728–734. doi: 10.1021/ed083p728

672   39 Dilruba S & Kalayda G V. (2016) Platinum-based drugs: past, present and future. *Cancer Chemother*
673   *Pharmacol* **77**, 1103–1124. doi: 10.1007/s00280-016-2976-z

674   40 Komeda S & Casini A (2012) Next-Generation Anticancer Metallodrugs. *Curr Top Med Chem* **12**, 219–235.
675   doi: 10.2174/156802612799078964

676   41 Zhang P & Sadler PJ (2017) Advances in the design of organometallic anticancer complexes. *J Organomet*
677   *Chem* **839**, 5–14. doi: 10.1016/j.jorganchem.2017.03.038

678   42 Anthony EJ, Bolitho EM, Bridgewater HE, Carter OWL, Donnelly JM, Imberti C, Lant EC, Lermyte F,
679   Needham RJ, Palau M, Sadler PJ, Shi H, Wang FX, Zhang WY & Zhang Z (2020) Metallodrugs are unique:
680   Opportunities and challenges of discovery and development. *Chem Sci* **11**, 12888–12917. doi:
681   10.1039/d0sc04082g

682   43 Jaouen G, Vessières A & Top S (2015) Ferrocifen type anti cancer drugs. *Chem Soc Rev* **44**, 8802–8817.
683   doi: 10.1039/c5cs00486a

684   44 Gasser G & Metzler-Nolte N (2012) The potential of organometallic complexes in medicinal chemistry. *Curr*
685   *Opin Chem Biol* **16**, 84–91. DOI: 10.1016/j.cbpa.2012.01.013

686   45 Szczepaniak A, Fichna J. (2019) Organometallic Compounds and Metal Complexes in Current and
687   Future Treatments of Inflammatory Bowel Disease and Colorectal Cancer-a Critical Review.
688   *Biomolecules*. **9**:398. doi: 10.3390/biom9090398.

689   46 Ndagi U, Mhlongo N & Soliman ME (2017) Metal complexes in cancer therapy – An update from drug
690   design perspective. *Drug Des Devel Ther* **11**, 599–616. doi: 10.2147/DDDT.S119488

691   47 Kostova I & Balkansky S (2013) Metal Complexes of Biologically Active Ligands as Potential Antioxidants.
692   *Curr Med Chem* **20**, 4508–4539. doi: 10.2174/09298673113206660288

693   48 Santini C, Pellei M, Gandin V, Porchia M, Tisato F & Marzano C (2014) Advances in copper complexes as
694   anticancer agents. *Chem Rev* **114**, 815–862. doi: 10.1021/cr400135x

695   49 Denoyer D, Clatworthy SAS, Cater MA. (2018) Copper Complexes in Cancer Therapy. Met Ions Life
696   Sci,18:/books/9783110470734/9783110470734-022/9783110470734-022.xml.
697   doi:10.1515/9783110470734-022

698   50 Marzano C, Pellei M, Tisato F & Santini C (2012) Copper Complexes as Anticancer Agents. *Anticancer*
699   *Agents Med Chem* **9**, 185–211. doi: 10.2174/187152009787313837

700   51 Shobha Devi C, Thulasiram B, Aerva RR & Nagababu P (2018) Recent Advances in Copper Intercalators as
701   Anticancer Agents. *J Fluoresc* **28**, 1195–1205. doi: 10.1007/s10895-018-2283-7

702   52 Liang X, Wu Q, Luan S, Yin Z, He C, Yin L, Zou Y, Yuan Z, Li L, Song X, He M, Lv C & Zhang W (2019)
703   A comprehensive review of topoisomerase inhibitors as anticancer agents in the past decade. *Eur J Med*
704   *Chem* **171**, 129–168. doi: 10.1016/j.ejmech.2019.03.034

705   53 Molinaro C, Martoriati A, Pelinski L & Cailliau K (2020) Copper complexes as anticancer agents targeting
706   topoisomerases i and ii. *Cancers (Basel)* **12**, 1–26. doi: 10.3390/cancers12102863

707 54 Wambang N, Schifano-Faux N, Aillerie A, Baldeyrou B, Jacquet C, Bal-Mahieu C, Bousquet T, Pellegrini
708   S, Ndifon PT, Meignan S, Goossens JF, Lansiaux A & Pélinski L (2016) Synthesis and biological activity
709   of ferrocenyl indeno[1,2-c]isoquinolines as topoisomerase II inhibitors. *Bioorganic Med Chem* **24**, 651–
710   660. doi: 10.1016/j.bmc.2015.12.033

711 55 Wambang N, Schifano-Faux N, Martoriati A, Henry N, Baldeyrou B, Bal-Mahieu C, Bousquet T, Pellegrini
712   S, Meignan S, Cailliau K, Goossens J-F, Bodart J-F, Ndifon PT & Pélinski L (2016) Synthesis, Structure,
713   and Antiproliferative Activity of Ruthenium(II) Arene Complexes of Indenoisoquinoline Derivatives.
714   *Organometallics* **35**. doi: 10.1021/acs.organomet.6b00440

715 56 Ahn G, Lansiaux A, Goossens JF, Bailly C, Baldeyrou B, Schifano-Faux N, Grandclaudon P, Couture A &
716   Ryckebusch A (2010) Indeno[1,2-c]isoquinolin-5,11-diones conjugated to amino acids: Synthesis,
717   cytotoxicity, DNA interaction, and topoisomerase II inhibition properties. *Bioorganic Med Chem* **18**,
718   8119–8133. doi: 10.1016/j.bmc.2010.08.025

719 57 Lewis KA, Lilly KK, Reynolds EA, Sullivan WP, Kaufmann SH & Cliby WA (2009) Ataxia telangiectasia
720   and rad3-related kinase contributes to cell cycle arrest and survival after cisplatin but not oxaliplatin. *Mol
721   Cancer Ther* **8**, 855–863. doi: 10.1158/1535-7163.MCT-08-1135

722 58 Wagner JM & Karnitz LM (2009) Cisplatin-induced DNA damage activates replication checkpoint signaling
723   components that differentially affect tumor cell survival. *Mol Pharmacol* **76**, 208–214. doi:
724   10.1124/mol.109.055178

725 59 Timofeev O, Cizmecioglu O, Settele F, Kempf T & Hoffmann I (2010) Cdc25 phosphatases are required for
726   timely assembly of CDK1-cyclin B at the G2/M transition. *J Biol Chem* **285**, 16978–16990. doi:
727   10.1074/jbc.M109.096552

728 60 Sur S, Agrawal DK. (2016) Phosphatases and kinases regulating CDC25 activity in the cell cycle: clinical
729   implications of CDC25 overexpression and potential treatment strategies. *Mol Cell Biochem*.416, 33-46.
730   doi: 10.1007/s11010-016-2693-2

731 61 Hans F & Dimitrov S (2001) Histone H3 phosphorylation and cell division. *Oncogene* **20**, 3021–3027. doi:
732   10.1038/sj.onc.1204326

733 62 Pommier Y. (2013) Drugging topoisomerases: lessons and challenges. *ACS Chem Biol*.**8**, 82-95. doi:
734   10.1021/cb300648v

735 63 Molinaro C, Martoriati A & Cailliau K (2021) Proteins from the DNA Damage Response: Regulation,
736   Dysfunction, and Anticancer Strategies. *Cancers (Basel)* **13**, 3819. doi: 10.3390/cancers13153819

737 64 Kondratskyi A, Kondratska K, Vanden Abeele F, Gordienko D, Dubois C, Toillon RA, Slomianny C,
738   Lemière S, Delcourt P, Dewailly E, Skryma R, Biot C & Prevarskaya N (2017) Ferroquine, the next
739   generation antimalarial drug, has antitumor activity. *Sci Rep* **7**, 1–15. doi: 10.1038/s41598-017-16154-
740   2

741 65 Lee SY, Kim CY & Nam TG (2020) Ruthenium complexes as anticancer agents: A brief history and
742   perspectives. *Drug Des Devel Ther* **14**, 5375–5392. doi: 10.2147/DDDT.S275007

743 66 Pragti, Kundu BK & Mukhopadhyay S (2021) Target based chemotherapeutic advancement of ruthenium
744   complexes. *Coord Chem Rev* **448**, 214169. doi: 10.1016/j.ccr.2021.214169

745 67 Dasari S & Bernard Tchounwou P (2014) Cisplatin in cancer therapy: Molecular mechanisms of action. *Eur

746   *J Pharmacol* **740**, 364–378. doi: 10.1016/j.ejphar.2014.07.025

747   68 Marzi L, Sun Y, Huang SYN, James A, Difilippantonio S & Pommier Y (2020) The indenoisoquinoline
748   LMP517: A novel antitumor agent targeting both TOP1 and TOP2. *Mol Cancer Ther* **19**, 1589–1597. doi:
749   10.1158/1535-7163.MCT-19-1064

750   69 Beck DE, Agama K, Marchand C, Chergui A, Pommier Y & Cushman M (2014) Synthesis and biological
751   evaluation of new carbohydrate-substituted indenoisoquinoline topoisomerase I inhibitors and improved
752   syntheses of the experimental anticancer agents indotecan (LMP400) and indimitecan (LMP776). *J Med*
753   *Chem* **57**, 1495–1512. doi: 10.1021/jm401814y

754   70 Ali Y & Abd Hamid S (2016) Human topoisomerase II alpha as a prognostic biomarker in cancer
755   chemotherapy. *Tumor Biol* **37**, 47–55. doi: 10.1007/s13277-015-4270-9

756   71 Zhong W, Yang Y, Zhang A, Lin W, Liang G, Ling Y, Zhong J, Yong J, Liu Z, Tian Z, Lin Q, Luo Q, Li Y
757   & Gong C (2020) Prognostic and predictive value of the combination of TOP2A and HER2 in node-
758   negative tumors 2 cm or smaller (T1N0) breast cancer. *Breast Cancer* **27**, 1147–1157. doi:
759   10.1007/s12282-020-01142-8

760   72 Barrett-Lee PJ, Dixon JM, Farrell C, Jones A, Leonard R, Murray N, Palmieri C, Plummer CJ, Stanley A &
761   Verrill MW (2009) Expert opinion on the use of anthracyclines in patients with advanced breast cancer at
762   cardiac risk. *Ann Oncol* **20**, 816–827. doi: 10.1093/annonc/mdn728

763   73 McGowan J V., Chung R, Maulik A, Piotrowska I, Walker JM & Yellon DM (2017) Anthracycline
764   Chemotherapy and Cardiotoxicity. *Cardiovasc Drugs Ther* **31**, 63–75. doi: 10.1007/s10557-016-6711-
765   0

766   74 Kinders RJ, Hollingshead M, Lawrence S, Ji U, Tabb B, Bonner WM, Pommier Y, Rubinstein L, Evrard YA,
767   Parchment RE, Tomaszewski J & Doroshow JH (2010) Development of a validated immunofluorescence
768   assay for γH2AX as a pharmacodynamic marker of topoisomerase I inhibitor activity. *Clin Cancer Res* **16**,
769   5447–5457. doi: 10.1158/1078-0432.CCR-09-3076

770   75 Marinello J, Delcuratolo M & Capranico G (2018) Anthracyclines as Topoisomerase II Poisons : From Early
771   Studies to New Perspectives. *Int J Mol Sci.* **19**, 3480. doi: 10.3390/ijms19113480

772   76 Dai Y & Grant S (2010) New insights into checkpoint kinase 1 in the DNA damage response signaling
773   network. *Clin Cancer Res* **16**, 376–383. doi: 10.1158/1078-0432.CCR-09-1029

774   77 Smith J, Mun Tho L, Xu N & A. Gillespie D (2010) The ATM-Chk2 and ATR-Chk1 pathways in DNA
775   damage signaling and cancer. *Adv Cancer Res.* **108**, 73-112. doi: 10.1016/B978-0-12-380888-2.00003-
776   0

777   78 Kuzminov A (2001) Single-strand interruptions in replicating chromosomes cause double-strand breaks. *Proc*
778   *Natl Acad Sci U S A* **98**, 8241–8246. doi: 10.1073/pnas.131009198

779   79 Saleh-Gohari N, Bryant HE, Schultz N, Parker KM, Cassel TN & Helleday T (2005) Spontaneous
780   Homologous Recombination Is Induced by Collapsed Replication Forks That Are Caused by Endogenous
781   DNA Single-Strand Breaks. *Mol Cell Biol* **25**, 7158–7169. doi: 10.1128/MCB.25.16.7158-7169.2005

782   80 Deng JH, Luo J, Mao YL, Lai S, Gong YN, Zhong DC & Lu TB (2020) Π-π stacking interactions: Non-
783   negligible forces for stabilizing porous supramolecular frameworks. *Sci Adv* **6**, 1–9. doi:
784   10.1126/sciadv.aax9976

785 81 Thakuria R, Nath NK & Saha BK (2019) The Nature and Applications of π-π Interactions: A Perspective.
786   *Cryst Growth Des* **19**, 523–528. doi: 10.1021/acs.cgd.8b01630

787 82 Atwal M, Swan RL, Rowe C, Lee KC, Armstrong L, Cowell IG, Austin CA & Lee DC (2019) Intercalating
788   TOP2 Poisons Attenuate Topoisomerase Action at Higher Concentrations s. **2019**, 475–484. doi:
789   10.1124/mol.119.117259

790 83 Pines J. (1999) Four-dimensional control of the cell cycle. *Nat Cell Biol.* **1**, E73-E79. doi: 10.1038/11041

791 84 Donzelli M & Draetta GF (2003) Regulating mammalian checkpoints through Cdc25 inactivation. *EMBO*
792   *Rep* **4**, 671–677. doi: 10.1038/sj.embor.embor887

793 85 Peng CY, Graves PR, Thoma RS, Wu Z, Shaw AS, Piwnica-Worms H. (1997) Mitotic and G2 checkpoint
794   control: regulation of 14-3-3 protein binding by phosphorylation of Cdc25C on serine-216. *Science* **277**,
795   1501-1505. doi: 10.1126/science.277.5331.1501

796 86 Shabbeer S, Omer D, Berneman D, et al. (2013) BRCA1 targets G2/M cell cycle proteins for ubiquitination
797   and proteasomal degradation. *Oncogene* **32**, 5005-5016. doi: 10.1038/onc.2012.522

798 87 Bassermann F, Eichner R, Pagano M. (2014) The ubiquitin proteasome system - implications for cell cycle
799   control and the targeted treatment of cancer. *Biochim Biophys Acta.* **1843**, 150-162. doi:
800   10.1016/j.bbamcr.2013.02.028

801 88 Bunz F, Dutriaux A, Lengauer C, et al. (1998) Requirement for p53 and p21 to sustain G2 arrest after DNA
802   damage. *Science.* **282**, 1497-1501. doi: 10.1126/science.282.5393.1497

803 89 Agarwal ML, Agarwal A, Taylor WR & Stark GR (1995) p53 controls both the G2/M and the G1 cell cycle
804   checkpoints and mediates reversible growth arrest in human fibroblasts. *Proc Natl Acad Sci U S A* **92**,
805   8493–8497. doi: 10.1073/pnas.92.18.8493

806 90 Chen J (2016) The cell-cycle arrest and apoptotic and progression. *Cold Spring Harb Perspect Biol*, **6**,
807   a026104. doi: 10.1101/cshperspect.a026104

808 91 Hermeking H, Lengauer C, Polyak K, et al. (1997) 14-3-3sigma is a p53-regulated inhibitor of G2/M
809   progression. *Mol Cell.* **1**, 3-11. doi: 10.1016/s1097-2765(00)80002-7

810 92 Borges HL, Linden R, Wang JY. (2008) DNA damage-induced cell death: lessons from the central nervous
811   system. *Cell Res.* **18**, 17-26. doi: 10.1038/cr.2007.110

812 93 Norbury CJ & Zhivotovsky B (2004) DNA damage-induced apoptosis. *Oncogene* **23**, 2797–2808. doi:
813   10.1038/sj.onc.1207532

814 94 Cheng Y, Ren X, Hait WN, Yang JM. (2013) Therapeutic targeting of autophagy in disease: biology and
815   pharmacology. *Pharmacol Rev.* **65**, 1162-97. doi: 10.1124/pr.112.007120.

816 95 Kinders RJ, Dull AB, Wilsker D, LeBlanc A, Mazcko C, Hollingshead MG,Parchment RE, Doroshow JH.
817   (2017) Antitumor activity of indenoisoquinoline inhibitors of topoisomerase 1 (TOP1) via apoptosis and
818   autophagocytosis pathways in animal models. *J. Clin. Oncol.*, **35**, 11588. doi:
819   10.1200/jco.2017.35.15_suppl.11588

820 96 Vega-Rubín-de-celis S (2020) The role of Beclin 1-dependent autophagy in cancer. *Biology (Basel)* **9**, 1–13.
821   doi: 10.3390/biology9010004

822 97 Kadowaki M & Karim MR (2009) *Chapter 13 Cytosolic LC3 Ratio as a Quantitative Index of*
823 *Macroautophagy*, 1st ed. Elsevier Inc. doi: 10.1016/S0076-6879(08)03613-6

824 98 Bjørkøy G, Lamark T, Pankiv S, Øvervatn A, Brech A & Johansen T (2009) Chapter 12 Monitoring
825 Autophagic Degradation of p62/SQSTM1. *Methods Enzymol* **451**, 181–197. doi: 10.1016/S0076-
826 6879(08)03612-4

827 99 Dunlop EA, Hunt DK, Acosta-Jaquez HA, Fingar DC & Tee AR (2011) ULK1 inhibits mTORC1 signaling,
828 promotes multisite Raptor phosphorylation and hinders substrate binding. *Autophagy* **7**, 737–747. doi:
829 10.4161/auto.7.7.15491

830 100 Ma Y, Vassetzky Y & Dokudovskaya S (2018) mTORC1 pathway in DNA damage response. *Biochim*
831 *Biophys Acta - Mol Cell Res* **1865**, 1293–1311. doi: 10.1016/j.bbamcr.2018.06.011

832 101 Young Chul K, Kun-Liang, G (2015). mTOR: a pharmacologic target for autophagy regulation. *Journal of*
833 *Clinical Investigation*, **125**, 25–32. doi: 10.1172/JCI73939

834 102 Abedin MJ, Wang D, McDonnell MA, Lehmann U, Kelekar A (2007) Autophagy delays apoptotic death in
835 breast cancer cells following DNA damage. Cell Death Differ. 14, 500–510. doi:10.1038/sj.cdd.4402039

836 103 Ma K, Chen G, Li W, Kepp O, Zhu Y, Chen Q (2020) Mitophagy, Mitochondrial Homeostasis, and Cell
837 Fate. *Front Cell Dev Biol*. **24**, 467. doi: 10.3389/fcell.2020.00467.

838 104 Tasdemir E, Maiuri MC, Galluzzi L, Vitale I, Djavaheri-Mergny M, D'Amelio M, Criollo A, Morselli E,
839 Zhu C, Harper F, Nannmark U, Samara C, Pinton P, Vicencio JM, Carnuccio R, Moll UM, Madeo F,
840 Paterlini-Brechot P, Rizzuto R, Szabadkai G, Pierron G, Blomgren K, Tavernarakis N, Codogno P, Cecconi
841 F, Kroemer G (2008) Regulation of autophagy by cytoplasmic p53. *Nat Cell Biol*. **10**, 676–87. doi:
842 10.1038/ncb1730

843 105 Leroy B, Girard L, Hollestelle A, Minna JD, Gazdar AF, Soussi T. (2014) Analysis of TP53 mutation status
844 in human cancer cell lines: a reassessment. *Hum Mutat*. 35, 756-765. doi:10.1002/humu.22556

845 106 Baptiste-Okoh N, Barsotti AM & Prives C (2008) Caspase 2 is both required for p53-mediated apoptosis
846 and downregulated by p53 in a p21-dependent manner. *Cell Cycle* **7**, 1133–1138. doi: 10.4161/cc.7.9.5805

847 107 Steinman RA & Johnson DE (2000) p21WAF1 prevents down-modulation of the apoptotic inhibitor protein
848 c-IAP1 and inhibits leukemic apoptosis. *Mol Med* **6**, 736–749. PMID: 11071269

849 108 Suzuki A, Tsutomi Y, Akahane K, Araki T & Miura M (1998) Resistance to Fas-mediated apoptosis:
850 Activation of caspase 3 is regulated by cell cycle regulator p21(WAF1) and IAP gene family ILP.
851 *Oncogene* **17**, 931–939. doi: 10.1038/sj.onc.1202021

852 109 Pattingre S, Tassa A, Qu X, Garuti R, Liang XH, Mizushima N, Packer M, Schneider MD, Levine B (2005)
853 Bcl-2 antiapoptotic proteins inhibit Beclin 1-dependent autophagy. *Cell*.122, 927-939.
854 doi:10.1016/j.cell.2005.07.002

855 110 Bursch W, Ellinger A, Kienzl H, Torok L, Pandey S, Sikorska M, Walker R, Hermann RS (1996) Active
856 cell death induced by the anti-estrogens tamoxifen and ICI 164 384 in human mammary carcinoma cells
857 (MCF-7) in culture: the role of autophagy.*Carcinogenesis* **17**, 1595–1607. doi: 10.1093/carcin/17.8.1595

858 111 Ogier-Denis E, Codogno P (2003) Autophagy: a barrier or an adaptive response to cancer. *Biochim Biophys*
859 *Acta* 1603, 113–128. doi: 10.1016/s0304-419x(03)00004-0.

860 112 Eich M, Roos WP, Nikolova T & Kaina B (2013) Contribution of ATM and ATR to the resistance of

861   glioblastoma and malignant melanoma cells to the methylating anticancer drug temozolomide. *Mol Cancer*
862   *Ther* **12**, 2529–2540. doi: 10.1158/1535-7163.MCT-13-0136

863   113 Jo U, Senatorov IS, Zimmermann A, Saha LK, Murai Y, Kim SH, Rajapakse VN, Elloumi F, Takahashi N,
864   Schultz CW, Thomas A, Zenke FT & Pommier Y (2021) Novel and Highly Potent ATR Inhibitor M4344
865   Kills Cancer Cells With Replication Stress, and Enhances the Chemotherapeutic Activity of Widely Used
866   DNA Damaging Agents. *Mol Cancer Ther*. **20**, 1431-1441. doi: 10.1158/1535-7163.MCT-20-1026

867   **12   Figure legends**

868   **Figure 1:** WN197 synthesis.

869   **Figure 2**: The copper complex WN197 induced DNA damage in cancer cells. MDA-MB-231, HeLa
870   and HT-29 cells were treated with DMSO (0.5%, solvent control), doxorubicin (5 µM, Top2 inhibitor
871   inducing DNA breaks), cisplatin (20 µM, alkylating agent inducing DNA breaks), WN170 (0.5 µM,
872   indenoisoquinoline without metal) or WN197 (0.5 µM). **(A)** Immunofluorescence of the DNA breaks
873   marker γH2AX was visualised as green *foci* in nuclei stained with DAPI (blue) on a Leica fluorescent
874   microscope 24 h after treatments. Images were representative of three independent experiments. Scale
875   bar : 20 µm **(B)** Quantification of γH2AX *foci* number per cells. **(C)** Western blot analysis of γH2AX
876   24 h after treatments. β-actin was used as a loading control and relative γH2AX level was quantified
877   by densitometry using Image J (Fiji Software, v1.52i). **(D)** Quantification of γH2AX *foci* number per
878   cells 30 min after treatments, based on immunofluorescence experiments. In B and D, data were
879   expressed as the mean ± SD for 30 nuclei of three independent experiments. Statistical analyses were
880   based on a two-way ANOVA followed by a Dunnett's test (**$p < 0,01$, ***$p < 0,005$ and ****$p < 0,001$).

881   **Figure 3**: WN197 inhibited human topoisomerase activity in a dose-dependent manner. (A) Top1
882   activity was determined by *in vitro* assays after addition of either DMSO (5%, solvent control, lane 4),
883   WN197 at different concentrations (0.2, 0.5, 1 and 2 µM, lanes 5-8), etoposide (VP-16, 50 µM; Top2
884   poison, lane 9) the negative control of Top1 activity inhibition, or camptothecin (CPT, 10 µM; Top1
885   poison, lane 10) the positive control of Top1 activity inhibition. Relaxed DNA (ᵣDNA, lane 1) or
886   supercoiled DNA (scDNA, lane 2) were used as migration controls. scDNA was used in all other
887   reactions in presence of Top1. The Top1 activity control allowing the relaxation of scDNA is in lane
888   3. The addition of proteinase K allowed detection of nicked DNA (ₙDNA), a witness of the single-
889   strand broken DNA stabilization by a topoisomerase poison. (B) Top2α activity inhibition assay.
890   Migration control of supercoiled DNA (scDNA) was performed in lane 1. Top2α was present in all
891   other reactions. The Top2α activity control for the relaxation of scDNA is in lane 2, the first band
892   corresponds to the transitional open circular DNA (ₒcDNA) and topoisomers correspond to the relaxed
893   DNA. DMSO (5%, solvent control) in lane 3, WN197 (concentrations of 0.2, 0.5, 1 and 2 µM) in lanes
894   4-7, etoposide (VP-16, 50 µM; Top2 poison) in lane 8, and camptothecin (CPT, 10 µM; Top1 poison)
895   in lane 9. (C) Top2β activity inhibition assay. Migration control of scDNA was performed in lane 1.
896   Top2β was present in all other reactions. The Top2β activity control for the relaxation of scDNA is in
897   lane 2, DMSO (5%, solvent control) in lane 3, WN197 (concentrations of 0.2, 0.5, 1 and 2 µM) in lanes
898   4-7, etoposide (VP-16, 50 µM; Top2 poison) in lane 8, and camptothecin (CPT, 10 µM; Top1 poison)
899   in lane 9. In (A), (B) and (C) after topoisomerase reactions, DNA was run in a 1% agarose gel, stained
900   with ethidium bromide (0.5 µg/mL), and visualized under UV light.

901   **Figure 4**: Activation of the DNA Damage Response (DDR) pathway. Cells were treated for 24 h with
902   doxorubicin (5 µM), cisplatin (20 µM), WN170 (0.5 µM), or WN197 (0.5 µM). Western blots were
903   performed to detect ATM, ATR, Chk1, Chk2, p53 and their phosphorylated forms, and p21. β-actin
904   was used as a loading control and relative protein levels were quantified by densitometry using Image
905   J software (Fiji Software, v1.52i). Results were representative of three independent experiments.

906 **Figure 5**: WN197 induced cell cycle accumulation in the G2/M phase. **(A)** Cytograms (G0/G1 and
907 G2/M first and second peaks respectively), and **(B)** flow cytometry analysis of MDA-MB-231, HeLa,
908 and HT-29 cells repartition in the cell cycle 24 h after treatments with cisplatin (20 µM, S phase arrest
909 control), nocodazole (84 nM, M phase arrest control), WN170 or WN197 (0.5 µM). **(C)** Dose-response
910 analysis by flow cytometry of G2/M phase accumulation 24 h after treatments with WN197. **(D)** Time
911 course analysis by flow cytometry of the cell cycle repartition in cell lines untreated (control) or treated
912 with WN197 (0.5 µM). Statistic were based on two-way ANOVA followed by Dunnett's test (*p<0,05,
913 **p<0,01, ***p<0,005 and ****p<0,001) on three independent experiments.

914 **Figure 6**: WN197 arrested the cell cycle in G2. **(A)** Western Blot analysis of cells treated for 24 h with
915 doxorubicin (5 µM), cisplatin (20 µM), WN170, WN197 (0.5 µM), or nocodazole (84 nM). β-actin
916 was used as a loading control. For H3 phosphorylation, respective H3 total levels were used as loading
917 controls. **(B)** 14-3-3 and Cdc25C immunoprecipitations were realized in cell lines treated for 24 h with
918 cisplatin (20 µM) or WN197 (0.5 µM). Relative protein levels were expressed by densitometry using
919 Image J software (Fiji Software, v1.52i). Results were representative of three independent experiments.

920 **Figure 7**: WN197-induced autophagy. Cells were treated for 24 h with doxorubicin (5 µM), cisplatin
921 (20 µM), WN170, WN197 (0.5 µM), nocodazole (84 nM) or rapamycin (0.5 µM). **(A)** Cleaved caspase
922 3 and PARP analysis by Western blots. Western blot analysis, after 3, 16, (24 or not), 48 and 72 h of
923 treatment with WN197 or doxorubicin for 24 and 48 h, of **(B)** cleaved PARP or **(C)** cytosolic
924 cytochrome C. **(D)** p62, Beclin-1, and LC3 markers analysis by Western blot. LC3 levels were
925 expressed upon the LC3-II/LC3-I ratio. β-actin levels were used as a loading control. Relative protein
926 levels were expressed by densitometry using Image J software (Fiji Software, v1.52i). **(E)** mTOR
927 immunoprecipitations were realized in cell lines untreated or treated with doxorubicin (5 µM),
928 rapamycin (0.5 µM) or WN197 (0.5 µM) for 24 h and followed by Western blots.

929 **Figure 8**: Deciphering of the molecular mechanisms of the novel copper(II) indenoisoquinoline
930 complex WN197. WN197 inhibits topoisomerases I at low doses in a poison mode and forms a ternary
931 complex with the topoisomerase and DNA, leading to strand breaks accumulation. Phosphorylated
932 H2AX (γH2AX) localizes at the sites of DNA damage. The DNA damage response pathway is
933 activated: ATM and ATR kinases are phosphorylated, and subsequently activate Chk1 and Chk2,
934 leading to Cdc25C phosphorylation on serine 216 (S216), and to its binding to 14-3-3. Consequently,
935 Cdk1 remains phosphorylated on tyrosine 15 (Y15), impeding the activation of the MPF (Cdk1/Cyclin
936 B) and the phosphorylation of H3 on serine 10 (S10). Cancer cells arrest in the G2 phase of the cell
937 cycle. The DDR also leads to an increase in p53 and p21 followed by an autophagic cell death
938 characterized by the phosphorylation of RAPTOR on serine 792 (S792) in the mTORC1 complex, the
939 synthesis of Beclin-1, the formation of LC3-II (complex LC3-I/PE (phosphatidylethanolamine)), and
940 the degradation of p62.

941 **Table 1**. Half maximal inhibitory concentrations (IC$_{50}$ in µM) for cell survival. *Data are expressed as*
942 *the mean ± SD of three independent experiments. Statistics were based on Student's t-test of the*
943 *difference between WN197 and WN170; ns: non-significative, **p<0.01 and ****p<0.0001.*

	MDA-MB-231	HeLa	HT-29
WN197	0.144 ± 0.01	0.220 ± 0.01	0.358 ± 0.07
WN170	$0.875 \pm 0,01$	0.630 ± 0.09	0.479 ± 0.07
Cisplatine	33.802 ± 1.27	19.287 ± 5.323	21.313 ± 7.475
Statistical difference (WN197/WN170)	****	**	*ns*

944

Table 2. Half maximal inhibitory concentrations (IC_{50} in μM) for cell survival of MCF-10A. *Data are expressed as the mean $\pm$ SD of three independent experiments. Statistics were based on Student's t-test of the difference between WN197 IC_{50} on adenocarcinomas and MCF-10A; ***p<0.001.*

Compound	IC_{50} (μM)
WN197	1.080 ± 0.037
Cisplatin	14.218 ± 7.157
Statistical difference (WN197 on adenocarcinomas vs. on MCF-10A)	***

948

Table 3. Melting curves and fluorescence measurements were determined for WN197 and WN170. *Variations in melting temperature ($\Delta Tm = Tm$ drug$-$DNA complex$-Tm$ DNA alone) were performed at a ratio of 0.5. Apparent binding constant were measured by fluorescence using [EB]/[DNA] = 1.26. Data were the mean of at least three independent experiments.*

Compound	ΔTm (°C)	Kapp (10^7 M-1)	EtBr displacement
WN197	16.6	15.005 ± 0.290	90%
WN170	16.1	2.436 ± 0.883	87%

953

954 **Supplementary data**

955 **S1:** Cytograms obtained after flow cytometry analysis of MDA-MB-231 cells 24 h after treatments or
956 not with WN197 (0.5 µM) or apoptosis positive control doxorubicin (5 µM, showing sub-G1
957 accumulation).

958 **S2**: Detection of apoptosis feature by annexin V-propidium iodide (PI). MDA-MB-231, HeLa, and
959 HT-29 cells were cultivated to 80% of confluence, incubated or not for 24 h with WN170 (0.5 µM),
960 WN197 (0.5 µM), camptothecin (20 µM; CPT) or doxorubicin (5 µM; Doxo), trypsinized, and washed
961 in ice-cold PBS. Cell suspensions were treated with PI and annexin V-FITC reagent (Apoptosis
962 Detection Kit, BD) using the manufacturer's protocol before they were analysed by flow cytometry
963 **(**CytoFLEX LX, Beckman Coulter**)** with Kaluza analysis software (v2.1.1). **(A)** Y-axis: number of PI-
964 stained cells. X-axis: number of annexin V-FITC-stained cells. The lower left quadrant represents non-
965 apoptotic cells (annexin V-FITC-negative and PI-negative cells; B--), the lower right quadrant
966 represents early apoptotic cells (annexin V-FITC-positive and PI-negative cells; B+-), the upper right
967 quadrant represents late apoptotic/necrotic cells (annexin V-FITC-positive and PI-positive cells; B++),
968 and the upper left quadrant represents prenecrotic cells (annexin V-FITC-negative and PI-positive
969 cells; B-+). **(B)** Representative histograms. Camptothecin and doxorubicin induced apoptosis in the
970 three cancer cell lines, while WN170 and WN197 had no effect compared to the control.
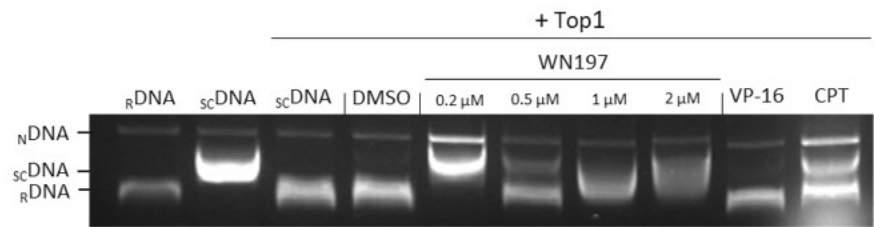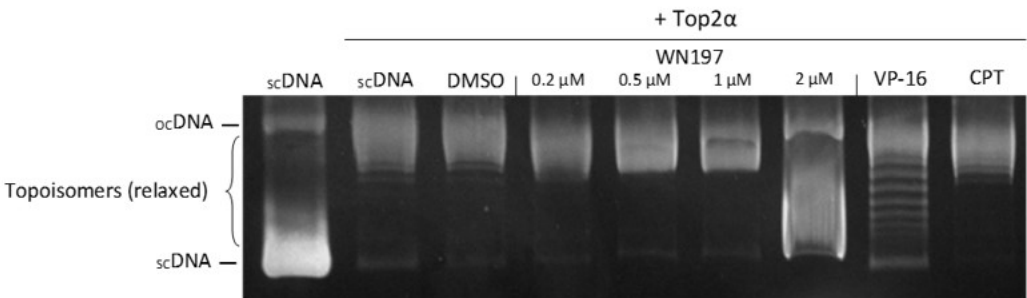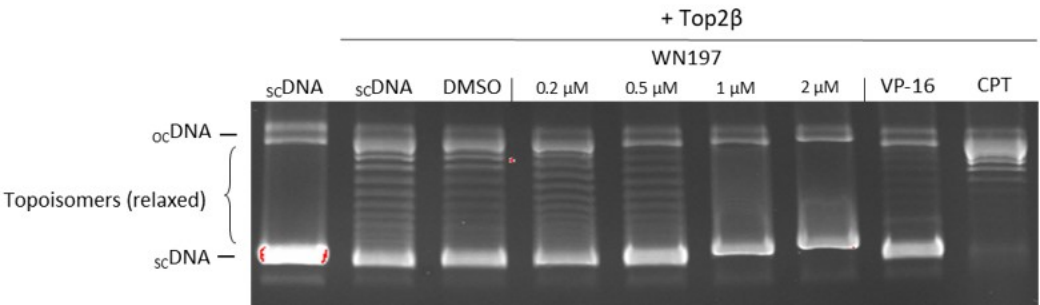
971

972

973 Figure 1

974

975

976
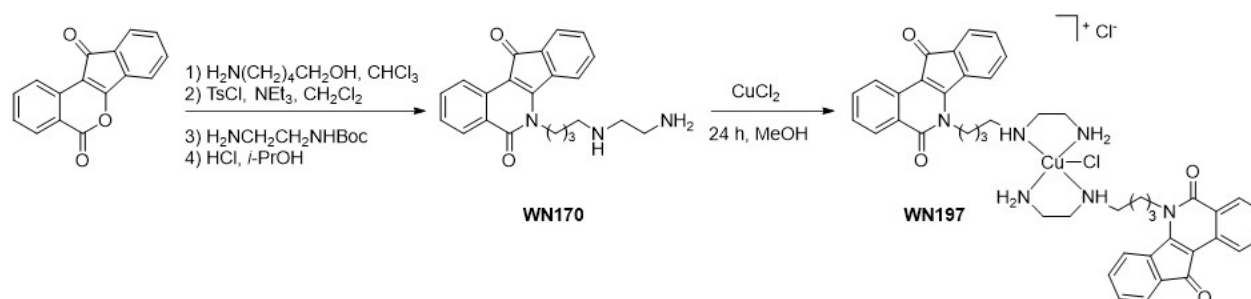
977   Figure 2
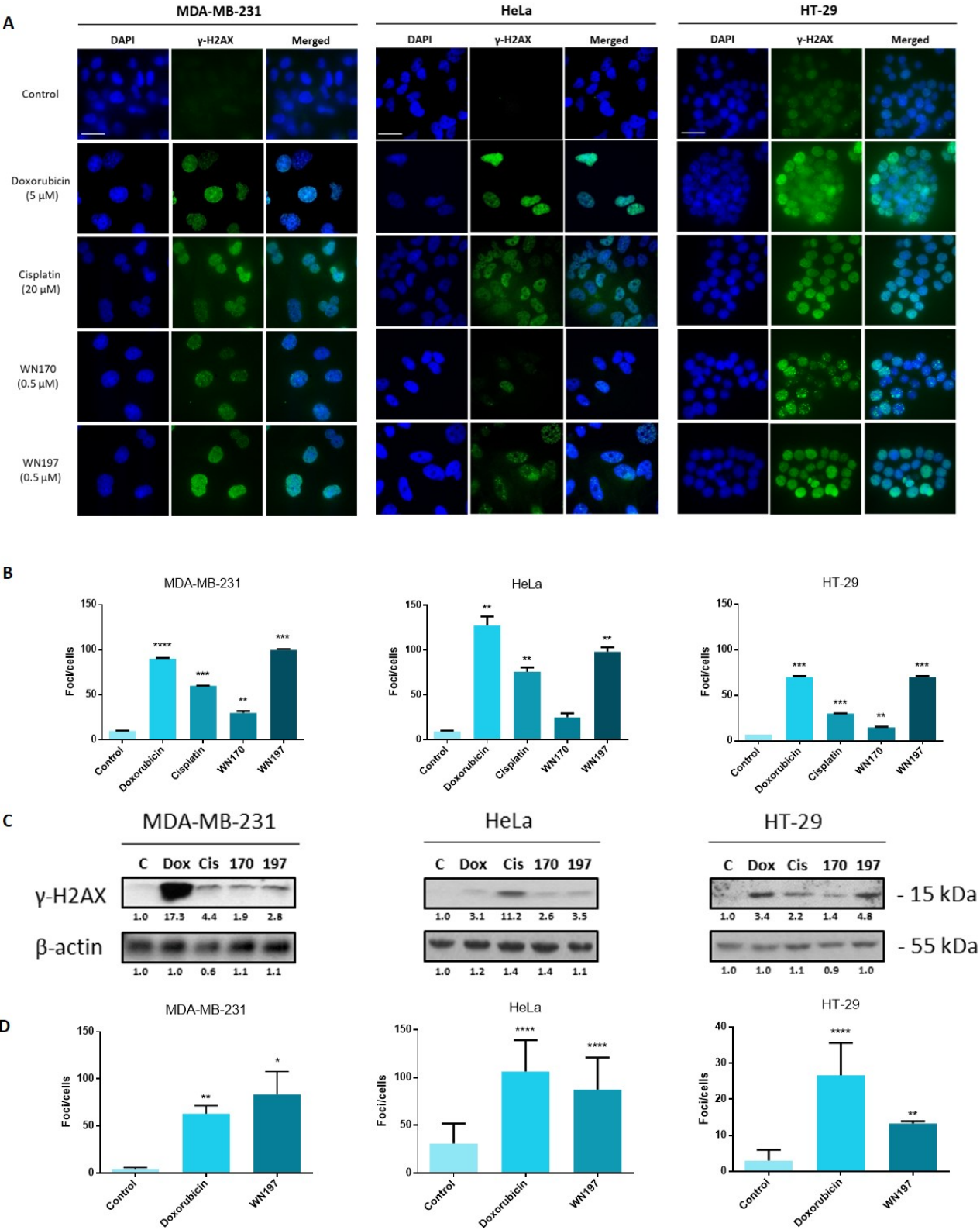
978

979

980   Figure 3

A

B

C

981

982

983   Figure 4

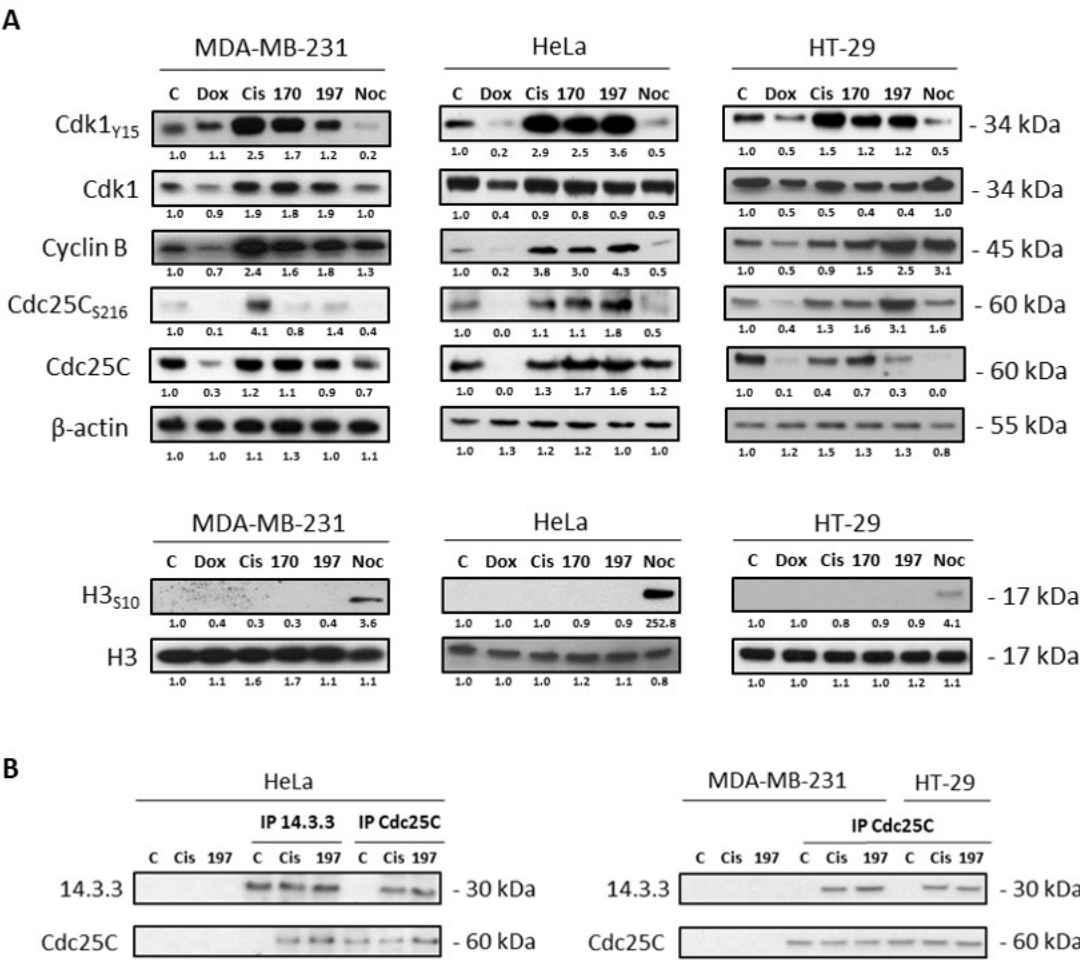|	MDA-MB-231	HeLa	HT-29
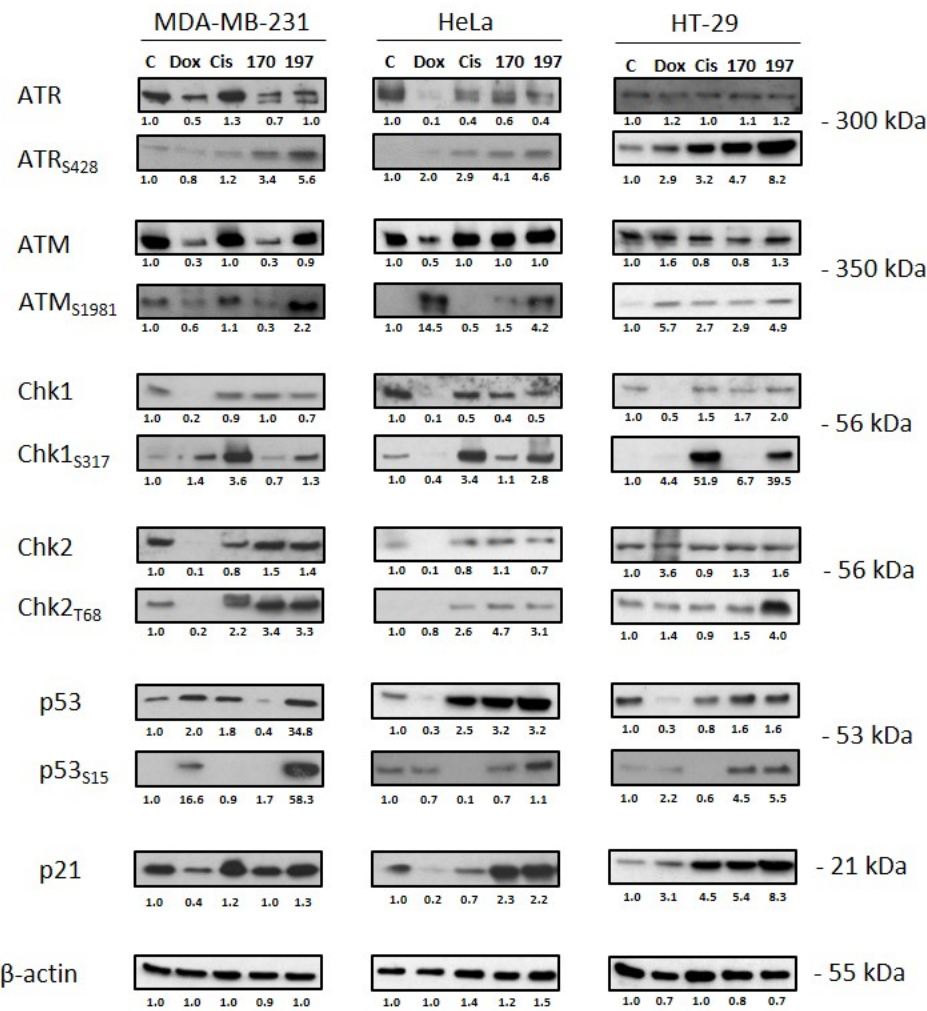
984

985

986   Figure 5
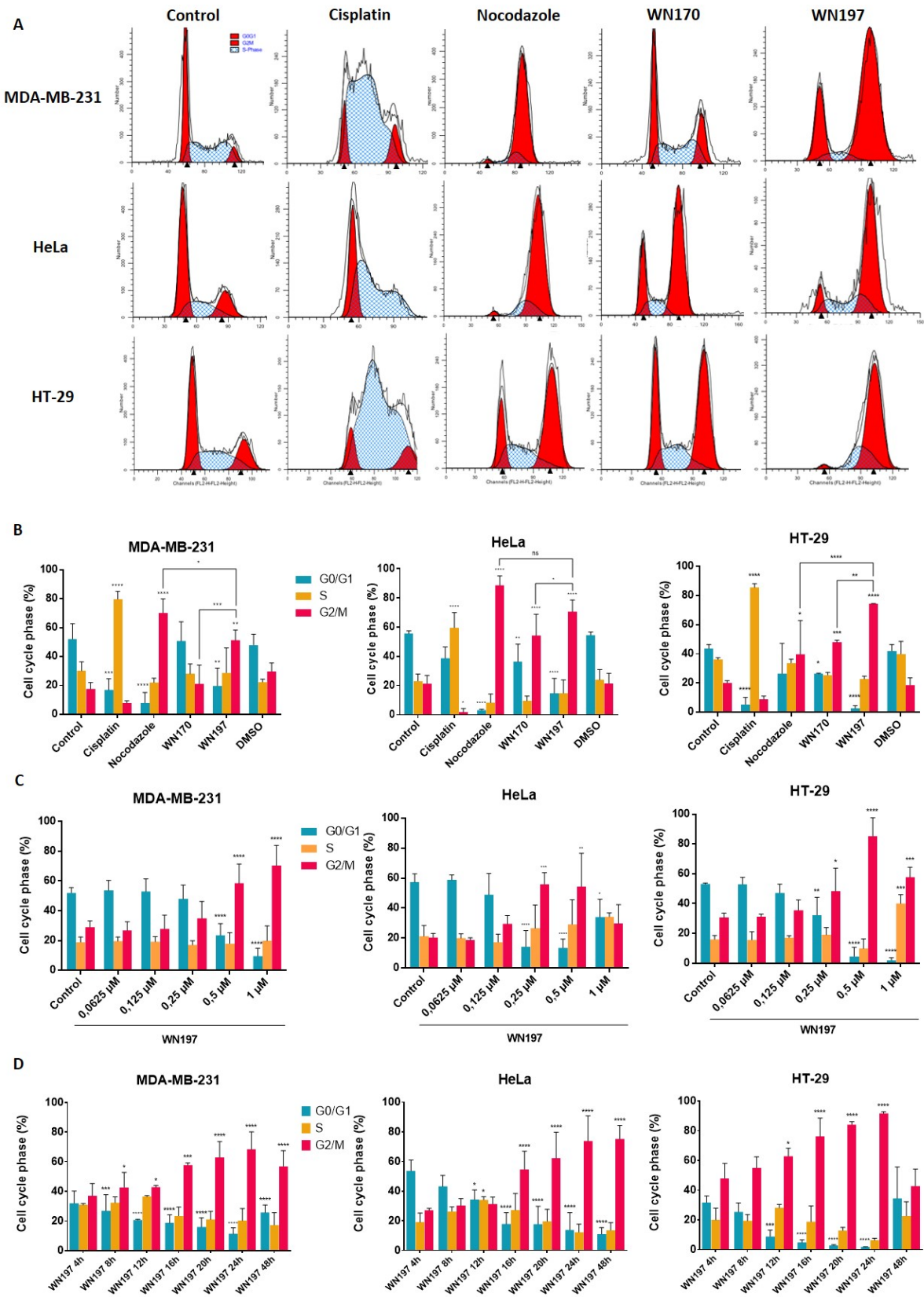
987

988

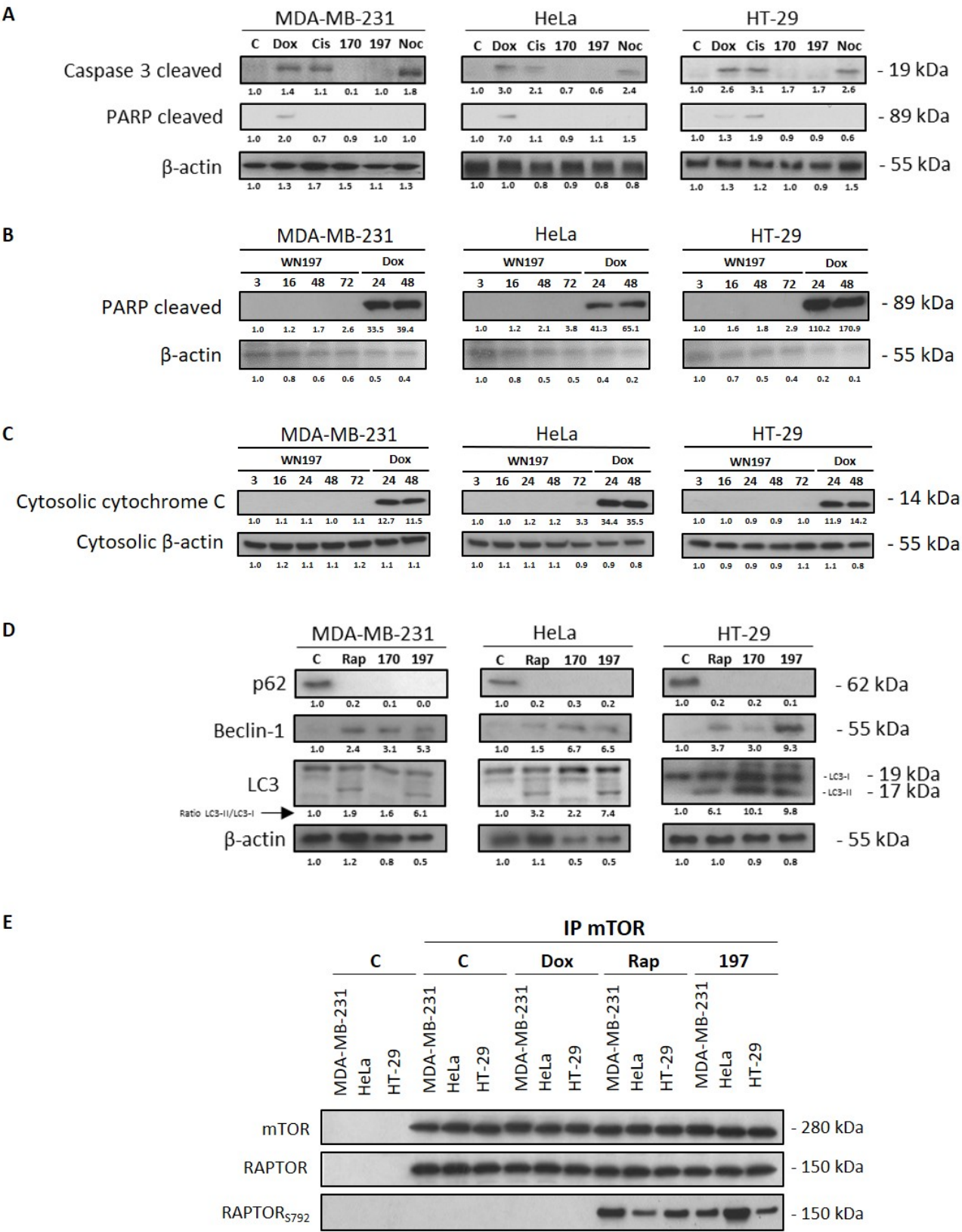989   Figure 6

A

990
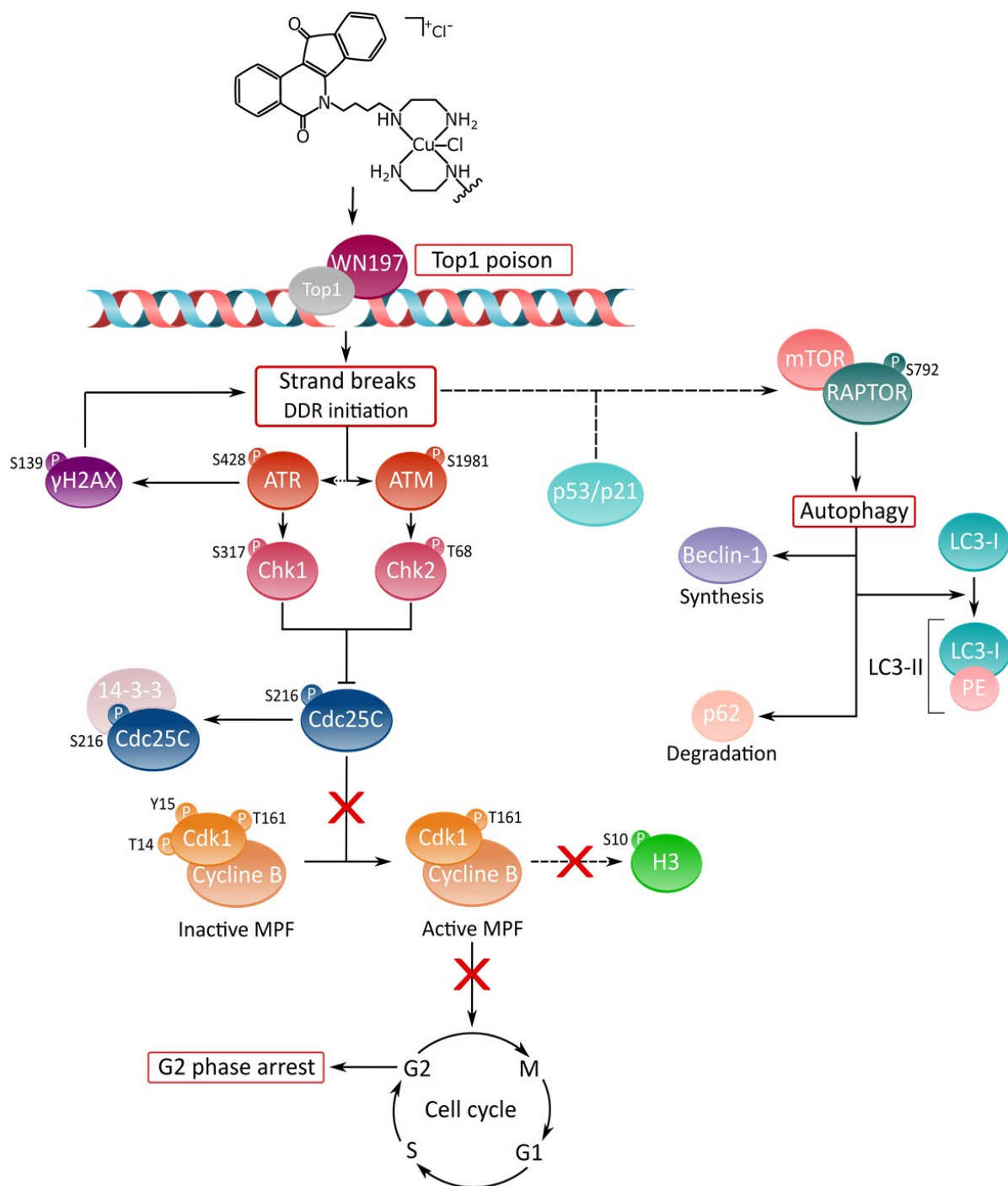
991

992   Figure 7

993

994

995   Figure 8
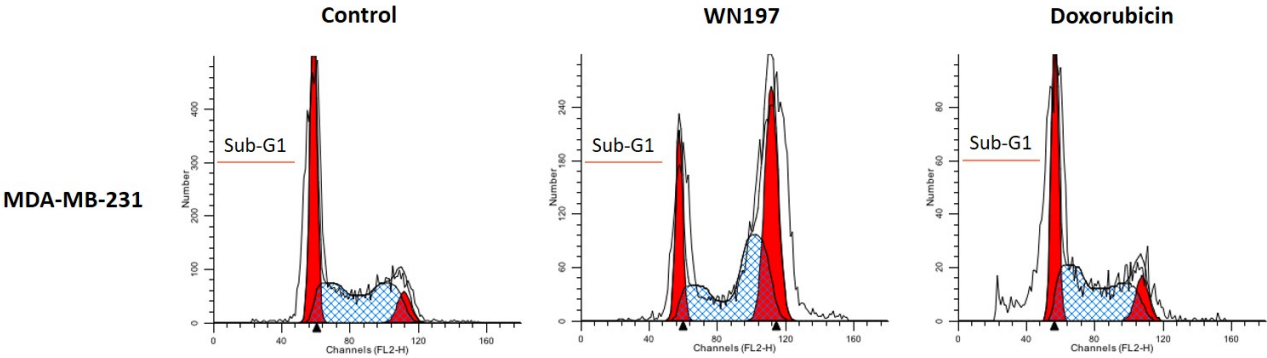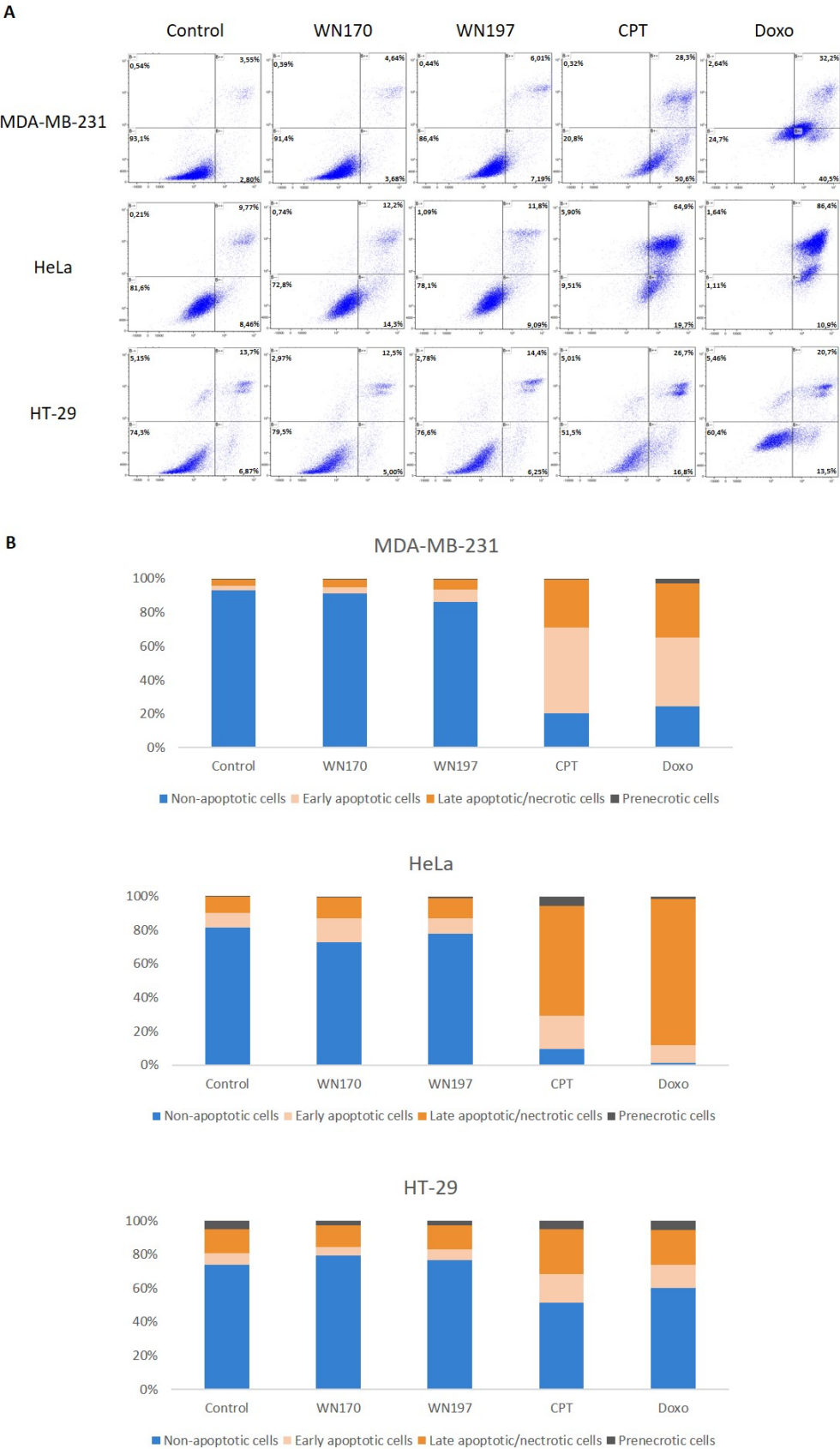
997   Supplementary DATA

998   Figure S1

999

1000

1001   Supplementary DATA.   Figure S2

1002